

Deanship of Graduate Studies
Al – Quds University



Analytical Study of Interaction between Two Penetrable Spheres

Ibrahim Abdul Kareem Salah

M.Sc. Thesis

Jerusalem – Palestine

1435 / 2014

Deanship of Graduate Studies
Al – Quds University



Analytical Study of Interaction between Two Penetrable Spheres

Prepared by:

Ibrahim Abdul Kareem Salah

Supervisor: Dr. Khawla Qamhieh

A thesis submitted in partial fulfillment of requirement for
the degree of Master of Science in Physics

Jerusalem – Palestine

1435/2014

Deanship of Graduate Studies
Al – Quds University



Thesis approval

Analytical Study of Interaction between Two Penetrable Spheres

Prepared by: Ibrahim Abdul kareem Salah
Registration No: 20714126

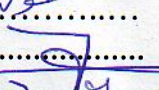
Supervisor: Dr. Khawla Qamhieh

Master thesis submitted and accepted, date 9/11/ 2014

The name and signature of examining committee member are as follows:

1. Head of the committee: Dr. Khawla Qamhieh
2. Internal Examiner: Dr. Imad Barghouthi
3. External Examiner: Dr. Jamal Ghabboun

Signature:

Signature:

Signature:

Jerusalem – Palestine

1435/2014

Dedication

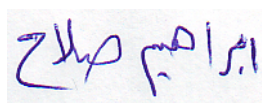
This thesis is dedicated to my parents. Also, this thesis is dedicated to my sister Safa'a and finally, this thesis is dedicated to all those who suffer from genetic problems and cancer.

Declaration

I hereby declare that this thesis is my own work and effort, and it has not been previously submitted by me anywhere for any university. Materials of work found by other researchers are mentioned in references.

The work was done under the supervision of Dr. Khawla Qamhieh, at Al – Quds University, Palestine.

Ibrahim Salah

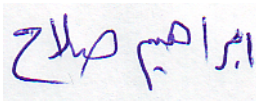


Acknowledgements

This thesis would not have been possible without the help, support and patience of my supervisor Dr. Khawla Qamhie. I would like to thank her, and also my faculties at Al Quds University.

My gratitude also goes to my friends, Mr. Azzam Abu Khalil, for his assistance, and to Christa Bryant for helping me in editing the English language. Thanks to my family and friends, who stood beside me and encouraged me constantly. Finally, alhamdulillah for making this thesis possible.

Ibrahim Salah



Abstract

The thesis's goal is to improve our understanding of the interaction between PAMAM dendrimer, dendrimer/DNA complex, dendrimer/DNA aggregate (many dendrimer/DNA complexes) and a soft particle like a cell or a protein in salt solution.

The electrostatic interactions between soft particles, such as dendrimers of different generations, or proteins, or cells, have been studied and calculated by implementing a new developed theoretical model derived by Ohshima. It describes the electrostatic interaction between two soft charged spheres during three stages: before penetration, through penetration, and after penetration.

It was found that the maximum interaction force between two interpenetrating soft spheres occurs in the second third of region of the full penetration (diameter of the smallest sphere). The electrostatic interaction decreases by increasing the concentration of the salt solution, but it is heavily dependent on the size of the particles when varying the concentration.

Interactions between dendrimer/DNA complexes, aggregates, and other soft particles are affected by the degree of the DNA wrapping around the dendrimer, and this wrapping length increases by the increasing of dendrimer generation.

This analytical study expands our understanding of the interaction between various soft particles in gene therapy.

Table of Contents

Title	Page
Abstract	iii
List of Tables	vi
List of Figures	vii
List of Abbreviations	xi
 Chapter One: Introduction	
1.1 Introduction	2
1.2 Dendrimers	3
1.3 Gene Therapy and Dendrimers	5
1.4 Previous studies	7
1.5 Theoretical model(Three stage model)	9
1.5.1 Electrostatic interactions between soft particles	9
1.5.2 Linearized Poisson-Boltzmann equations for two interacting charged porous spheres (soft spheres)	10
1.5.2.1 Stage 1: Interaction between two porous spheres before contact	15
1.5.2.2 Stage 2: Interaction between two partially interpenetrating charged porous Spheres	16
1.5.2.3 Stage 3: Interaction for the case where sphere 2 is engulfed by sphere 1	18
1.6 Statement of the problem	20
 Chapter Two: The Model and Method	
2.1 Introduction	22
2.2 Electrostatic interaction energy and force before the penetration	22
2.3 Electrostatic interaction energy and force during the penetration	22
2.4 Electrostatic interaction energy and force after the penetration	23
2.5 Simplification	23
 Chapter Three: Results and Discussions	
3.1 Introduction	26
3.2 Effect of some parameters on interaction between two soft spheres	26
3.2.1 Effect of the particle's charge on the electrostatic interaction	26

3.2.2Size effect on the electrostatic interaction between two soft charged spheres	28
3.2.3.1 Effect of monovalent salt concentration measured by inverse Debye length (κ)	31
3.2.3.2 Effect of ion's valence of the salt on the interaction between two soft interpenetrating charged spheres	37
3.2.4 Effect of Bjerrum length l_B on the interaction	40
3.2.4.1 Effect of Relative permittivity ϵ_r on the interactions under fixed temperature	40
3.2.4.2 Effect of temperature on interactions under fixed dielectric constants	46
3.3 The interaction of a soft sphere with two different types of PAMAM dendrimers	50
3.4 Interactions of Complex DNA/ G_n with soft charged particles	53
3.5 Interaction of a soft sphere with Aggregates	57
 Chapter Four : Conclusion and Future Work	
Conclusion and Future Work	61
References	64

List of Tables

Table 1.1	Theoretical properties of Ethlenediamine Cored and Ammonia Cored PAMAM dendrimers.	5
Table 3.1	The ratio B represents the location of the maximum force point $[R_{max} - (a_1 - a_2)]$ to the length of penetration interval $(2 a_2)$, where a_1, a_2 are radii of sphere 1 and sphere2 respectively.	30
Table 3.2	The measured values of l_B in nm unit correspond to some selected ϵ_r values at room temperature.	41
Table 3.3	Measured values of l_B under fixed relative permittivity value of water at $\epsilon_r = 80$.	47
Table 3.4	The calculated net charge of complexes G_4/DNA and G_6/DNA , l takes the values :20,50,100,150,and 200 nm , where Z_4^* is the net charge of the G_4/DNA complex and Z_6^* is the net charge of the G_6/DNA complex	53
Table 3.5	The calculated approximate radius of the aggregate of $N G_n/\text{DNA}$ complexes, where Z^* is the net charge on the aggregate, the Z^* and N values were obtained from previous study (Qamhieh et al., 2014).	58

List of Figures

Figure 1.1	Structure of (a) Polyamidoamine (PAMAM) dendrimer, and (b) Generation (G_3) of dendrimer	4
Figure 1.2	a) Complex structure b) Forming aggregate	6
Figure 1.3	Nucleosome structure	7
Figure 1.4	The three stages of interaction between two soft charged spheres	9
Figure 1.5	The fixed-charge density ρ in the respective regions in the three stages a) Stage 1 b) Stage 2 c) Stage 3	12
Figure 3.1	Interactions measurements between soft sphere1 ($a_1 = 10\text{nm}$, $Z_1 = 100$), and soft sphere2 ($a_2 = 5\text{nm}$) where $Z_2 = 1, 10, 20, 50$, and 100 for each case (a) Interaction energy V as a function of distance R (b) The interaction force as a function of distance R for each case of (a)	27
Figure 3.2	R_{max} versus Z , where R_{max} is the distance R at the maximum interaction force value P_{max}	28
Figure 3.3	(a) Interaction energy where $a_1 = 10\text{ nm}$ and $a_2 = 1\text{nm}, 4\text{nm}, 6\text{nm}, 8\text{nm}, 10\text{nm}$; in all cases $Z_1 = Z_2 = 10$, $l_B = 0.7\text{nm}$, and the salt concentration $= 10\text{m}$. (b) The interaction force versus distance R for each case	29
Figure 3.4	(a) The distance R at the maximum interaction force versus a_2 in nm unit. (b) The ratio B [distance of R_{max} from lower term of penetration interval ($a_1 - a_2$) to length of penetration interval ($2a_2$), which is bounded by upper term ($a_1 + a_2$) and lower term ($a_1 - a_2$)], versus the radius of sphere 2 in nm.	30
Figure 3.5	The interaction energy $V(R)$ of a sphere with radius $a = 10\text{nm}$ and $Z = 10000$ immersed in Monovalent aqueous solution ($l_B = 0.7$) takes different concentration values $0.1, 0.4, 1.1, 2.8, 5.6, 10.1\text{mM}$ interacts with (a) G_2 (b) G_4 (c) G_6 (d) G_8	32
Figure 3.6	The interaction force $P(R)$ of a sphere with radius $a = 10\text{nm}$ and $Z = 10,000$ immersed in monovalent aqueous solution ($l_B = 0.7$) takes concentration values $0.1, 0.4, 1.1, 2.8, 5.6, 10.1\text{mM}$ interacts with (a) G_2 (b) G_4 (c) G_6 (d) G_8 .	33
Figure 3.7	The maximum interaction force P_{max} versus Concentration C in mM unit when a sphere with 10nm radius and number Charge $Z = 10,000$ interacts with (a) G_2 (b) G_4 (c) G_6 (d) G_8 .	34

Figure 3.8	The interaction energy $V(R)$ of a sphere with radius $a=1,000\text{nm}$ and $Z=10,000$ immersed in a monovalent aqueous solution ($l_B=0.7$) taking concentration values 0.1, 0.4, 1.1, 2.8, 5.6, 10.1mM interacts with (a) G_2 (b) G_4 (c) G_6 (d) G_8	35
Figure 3.9	The interaction force $P(R)$ of a sphere with radius $a=1,000\text{nm}$ and $Z=10,000$ immersed in a monovalent aqueous solution ($l_B=0.7$) taking concentration values 0.1, 0.4, 1.1, 2.8, 5.6, 10.1mM interacts with (a) G_2 (b) G_4 (c) G_6 (d) G_8	36
Figure 3.10	The maximum interaction force P_{max} versus Concentration C in mM unit when a sphere with 1,000nm radius and charge number $Z=10,000$ interacts with (a) G_2 (b) G_4 (c) G_6 (d) G_8	37
Figure 3.11	Interaction energy of a sphere with 10nm radius and $Z=10,000$ immersed in three solutions, having the same salt concentration 10mM and $l_B=0.7$ but various values of valence ions in each solution $z = 1,2,3$ interacting with (a) G_2 (b) G_4 (c) G_6 (d) G_8	38
Figure 3.12	Interaction force of a sphere with 10nm radius and $Z=10000$ immersed in three solutions having the same salt concentration 10mM and $l_B=0.7$ but various values of valence ions in each solution $z = 1,2,3$ interacting with (a) G_2 (b) G_4 (c) G_6 (d) G_8	39
Figure 3.13	The interaction energy $V(R)$ of a sphere with radius $a=10\text{nm}$ and $Z=10,000$ immersed in a monovalent aqueous solution with 10mM concentration and Bjerrum length takes different values $l_B= 0.6, 0.65, 0.7, 0.75, 0.8, 0.85, 0.9\text{nm}$ in each case at room temperature interacts with (a) G_2 (b) G_4 (c) G_6 (d) G_8	41
Figure 3.14	The interaction force $P(R)$ of a sphere with radius $a=10\text{nm}$ and $Z=10,000$ immersed in an Monovalent aqueous solution with 10mM concentration and Bjerrum length takes different values $l_B= 0.6, 0.65, 0.7, 0.75, 0.8, 0.85, 0.9\text{nm}$ in each case at room temperature interacts with (a) G_2 (b) G_4 (c) G_6 (d) G_8	42
Figure 3.15	The maximum interaction force P_{max} versus Bjerrum length l_B in (nm) unit when a sphere with 10nm radius and Charge number $Z=10,000$ interacts with (a) G_2 (b) G_4 (c) G_6 (d) G_8	43
Figure 3.16	The interaction energy $V(R)$ of a sphere with radius $a=1,000\text{nm}$ and $Z=10,000$ immersed in a monovalent aqueous solution with 10mM concentration and Bjerrum length taking different values $l_B= 0.6, 0.65, 0.7, 0.75, 0.8, 0.85, 0.9\text{nm}$ in each case at room temperature interacts with (a) G_2 (b) G_4 (c) G_6 (d) G_8	44

Figure 3.17	The interaction force $P(R)$ of a sphere with radius $a = 1,000\text{nm}$ and $Z=10,000$ immersed in a monovalent aqueous solution with 10mM concentration and Bjerrum length taking different values $l_B = 0.6, 0.65, 0.7, 0.75, 0.8, 0.85, 0.9\text{nm}$ in each case at room temperature interacts with (a) G_2 (b) G_4 (c) G_6 (d) G_8	45
Figure 3.18	The maximum interaction force P_{max} versus Bjerrum length l_B in (nm) unit for a sphere with 1000nm radius and charge number $Z=10,000$ interacts with (a) G_2 (b) G_4 (c) G_6 (d) G_8	46
Figure 3.19	The interaction energy $V(R)$ of a sphere with radius $a = 10\text{nm}$ and $Z=10,000$, immersed in an monovalent aqueous solution with 10mM concentration at different values of temperature in Kelvin in each case, interacts with (a) G_2 (b) G_4 (c) G_6 (d) G_8	47
Figure 3.20	The interaction force $P(R)$ of a sphere with radius $a = 10\text{nm}$ and $Z=10,000$, immersed in an monovalent aqueous solution with 10mM concentration at different values of temperature in Kelvin in each case, interacts with (a) G_2 (b) G_4 (c) G_6 (d) G_8	48
Figure 3.21	The maximum interaction force P_{max} of a sphere with radius $a = 10\text{nm}$ and $Z=10,000$, immersed in an monovalent aqueous solution with 10mM concentration at different values of temperature in Kelvin in each case, interacts with (a) G_2 (b) G_4 (c) G_6 (d) G_8	49
Figure 3.22	The interaction energy $V(R)$ of a sphere with radius $a = 10\text{ nm}$ and $Z=10,000$ immersed in an monovalent aqueous solution ($l_B=0.7$) and 10mM Salt concentration interacts with G_2, G_4, G_6, G_8 and G_{10} of (a) Ethylenediamine cored PAMAM dendrimer (b) Ammonia cored PAMAM dendrimer (c) Interaction force $P(R)$ for each case of (a) (d) Interaction force $P(R)$ for each case of b	51
Figure 3.23	The interaction energy $V(R)$ of a sphere with radius $a = 1,000\text{nm}$ and $Z=10,000$ immersed in a monovalent aqueous solution ($l_B=0.7$) and 10mM salt concentration interacts with generations G_2, G_4, G_6, G_8 and G_{10} of (a) Ethylenediamine cored PAMAM dendrimer (b) Ammonia cored PAMAM dendrimer (c) Interaction force $P(R)$ for each case of a (d) Interaction force $P(R)$ for each case of b	52
Figure 3.24	The interaction energy of a charged sphere has radius $a = 10\text{nm}$ and $Z=10,000$ immersed in an monovalent aqueous solution ($l_B=0.7$) and 10mM salt concentration interacts with (a) Complex G_4/DNA when wrapping length of DNA (l) takes different values (b) Complex G_6/DNA (c) The interaction force in each case of a (d) The interaction force in each case of b	55

- Figure 3.25 The interaction energy of a charged sphere has radius $a = 1,000\text{nm}$ and $Z=10,000$ immersed in an monovalent aqueous solution ($l_B=0.7$) and 10mM salt concentration interacts with (a) Complex G_4/DNA when wrapping length of DNA (l) takes different values. (b) Complex G_6/DNA (c) The interaction force in each case of a (d) The interaction force in each case of b 56
- Figure 3.26 (a) The interaction energy of a charged sphere of radius $a = 50\text{nm}$ and $Z=10,000$ immersed in monovalent aqueous solution ($l_B=0.7$) with 10mM salt concentration interacts with different generation of aggregates (b)The interaction force in each case of a 58
- Figure 3.27 (a) The interaction energy of charged sphere of radius $a = 1000\text{nm}$ and $Z=10,000$ immersed in a monovalent aqueous solution ($l_B=0.7$) with 10mM salt concentration interacts with different generations of aggregates (b) The interaction force in each case of a 59

List of abbreviations

DNA	Deoxyribonucleic acid
G_n	Generation(n) of dendrimer
PAMAM	Poly(amido amine)
E.C.P	Ethlenediamine Cored PAMAM dendrimer
A.C.P	Ammonia Cored PAMAM dendrimer
b	Spacing between phosphate groups in DNA
l_B	Bjerrum length
l	Wrapping length of DNA
Z_{dend}	Number of functional groups of dendrimer
Z_{compl}	The net charge of the complex

Chapter One

Introduction

Chapter One

1.1 Introduction

Over the past few decades, there has been great interest in developing biodegradable nanoparticles (generally vary in size from few to 1000 nm) as effective drug delivery for medical applications. One of the related experimental techniques is gene therapy, which uses DNA(deoxyribonucleic acid) as a drug to treat disease by delivering therapeutic DNA into a patient's cells.

A delivery vehicle (vector), of either viral or non-viral origin, must be used to carry the foreign gene into a cell. Viral vectors take advantage of the facile integration of the gene of interest into the host and high probability of its long-term expression, but are plagued by safety concerns. Non-viral vectors, although less efficient at introducing and maintaining foreign gene expression, have the profound advantage of being non-pathogenic and non-immunogenic. Polycation–DNA complexes are particularly attractive for non-viral gene therapy (Thomas and Klibanov, 2003).

In gene therapy technique, the packing pathway of DNA inside the nucleus of a cell is still matter of great debate. Recently, many effective materials in nano scale have emerged for delivering DNA, including several nonviral vectors, namely, liposomes, lipospermines, polycationic lipids...etc. (Eichman et al., 2000).

Dendrimer is one of these materials, capable of condensing DNA to nanoparticles with radii of 20-100 nm. Dendrimer can have a positive charge; the negative DNA wraps around the positive dendrimer to form dendrimer /DNA complex. Qamhieh and co-workers provided further insights into the formation and structure of complexes and aggregates of different generations by applying a relatively simple analytical model (Qamhieh et al., 2014).

In nature, important ions and nanometer-sized proteins are transported across the lipid bilayer through specialized membrane-transport protein channels. The efficient passage of drugs through the plasma membrane remains a major hurdle for drug delivery. Cellular uptake is a complex mechanism and involves several important factors that include concentration of penetrating material across the cell membrane, surface charge, and hydrogen bonding with the cell membrane (Patil et al., 2008). Good cell uptake often requires the administration of high quantities of drugs in order to obtain the expected intracellular biological effect. The interaction of nanomaterial with cells and lipid bilayers and how the nanoparticle surface (in addition to nanoparticle shape and size) impact their interaction with lipid bilayers and cells were studied (Verma and Stellacci, 2009). Other researchers have been studying the mechanism of dendrimer-mediated cell entry and simulations of dendrimers with lipid bilayers (Eichman et al.,2000; Lee and Larson, 2009).

If dendrimers are to deliver drugs and other useful molecules into cells, they must first interact with the cell membrane and then interact inside the cell. Here, to improve the gene delivery into cells and into the nuclei, the interactions must be understood in intervals; before penetration, during the penetration process and after the penetration.

1.2 Dendrimers :

Dendrimers are branched polymers that consist of a central core as Ammonia and Ethylenediamine cores, repeated building blocks, and many surface terminal groups, as shown in Figure 1.1 (Lee and Larson, 2009).

The first dendrimers were made by divergent synthesis approaches , then a convergent synthetic approach was introduced. (Buhleier et al., 1978; Hawker and Frechet, 1990).

Dendrimers have a controlled mass, uniform structure, surface functionality, and good water solubility. Dendrimers have been studied for many biomedical applications such as antitumor therapeutics and drug delivery as previously mentioned. Drugs, sensing and molecules can be attached to the dendrimer, and those complexes can be targeted to the specific cancer cells (Lee and Larson, 2009). Dendrimers are classified by generation G_n , which refers to the number (n) of repeated branching cycles that are performed during its synthesis, for example if a dendrimer is made by convergent synthesis as in Figure 1.1 , and the branching reactions are performed onto the core molecule three times, the resulting dendrimer is considered a third generation dendrimer G_3 . Each successive generation G_n results in a dendrimer roughly twice the molecular weight of the previous generation G_{n-1} . Higher generation dendrimers have more exposed functional groups on the surface, which can later be used to customize the dendrimer for a given application. (Holister et al., 2003)

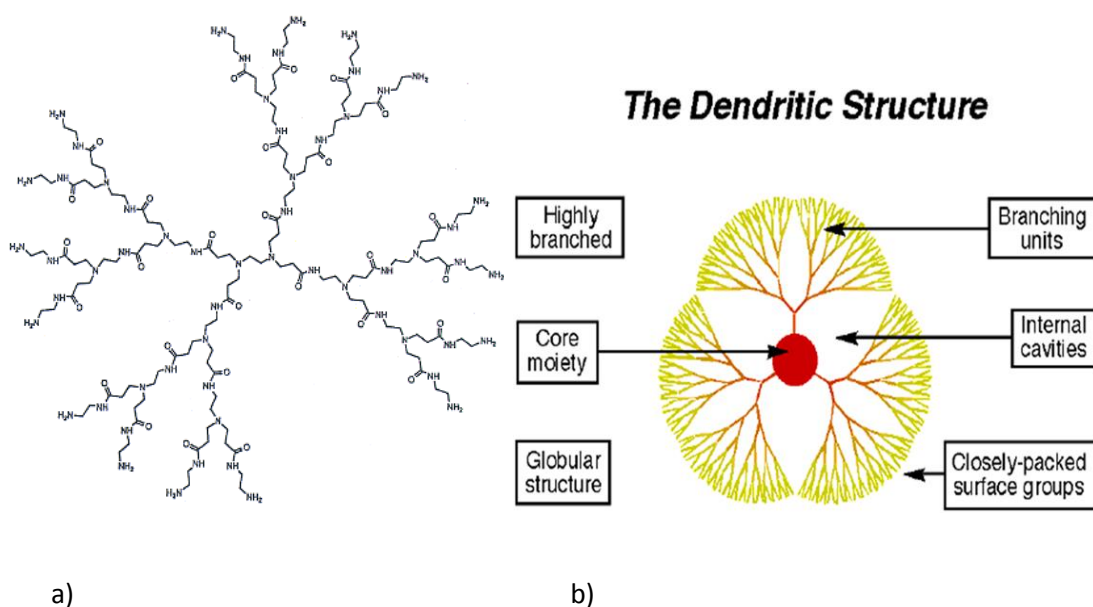


Figure 1.1: Structure of (a) Polyamidoamine (PAMAM) dendrimer, and (b) Generation (G_3) of dendrimer. Image reproduced from <http://nano.med.umich.edu>

The dendrimers are also named by the core group. Table (1.1) shows two types of dendrimers and some of their theoretical properties.

Table 1.1: Theoretical properties of Ethylenediamine Cored and Ammonia Cored PAMAM dendrimers (Bruckman et al., 2013).

Generation	Measured Diameter (Å)		Surface Groups	
	Ethylenediamine cored	Ammonia cored	Ethylenediamine cored	Ammonia cored
0	15	11	4	3
1	22	16	8	6
2	29	22	16	12
3	36	31	32	24
4	45	40	64	48
5	54	54	128	96
6	67	68	256	192
7	81	84	512	384
8	97	95	1024	768
9	114	107	2048	1536
10	135	124	4096	3072

1.3 Gene Therapy and Dendrimers :

In gene therapy and drug delivery fields, dendrimers have been used as vehicles, as transporters to increase their targeting efficiency. The interactions of dendrimers with lipid bilayers, DNA (deoxyribonucleic acid), and other molecules and particles have been the subject of many studies. Although experiments have provided vital information on the large-scale interactions between dendrimers and other molecules, many atomic-level questions that cannot be answered by experiments remain to be solved.

Therefore, theoretical and computational modeling methods have been applied to investigate the atomic-scale insights into the interactions of dendrimers with other molecules and particles (Lee and Larson, 2009), such as interaction of dendrimers with DNA. Native DNA consists of double chains, each chain consists of charged repeated groups. One of them is a phosphate group and has a net negative charge and there is spacing (b) between phosphate groups $b= 0.17\text{nm}$. Like other poly ions in aqueous solutions, DNA interacts with oppositely charged poly-electrolytes (dendrimers) DNA wraps on the positive dendrimers to form interpolyelectrolyte complexes (Kabanov et al., 2000) as shown in Figure 1.2a, and complexes together produce aggregate structure, as shown in Figure 1.2b.

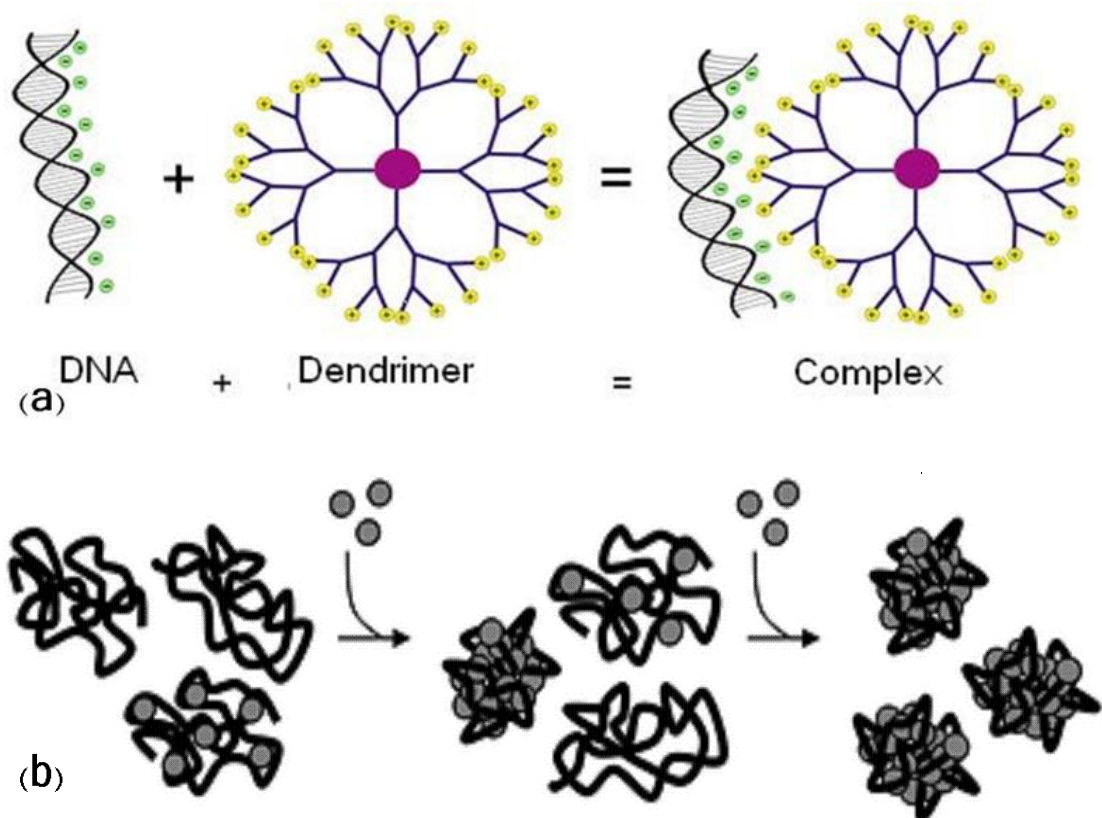
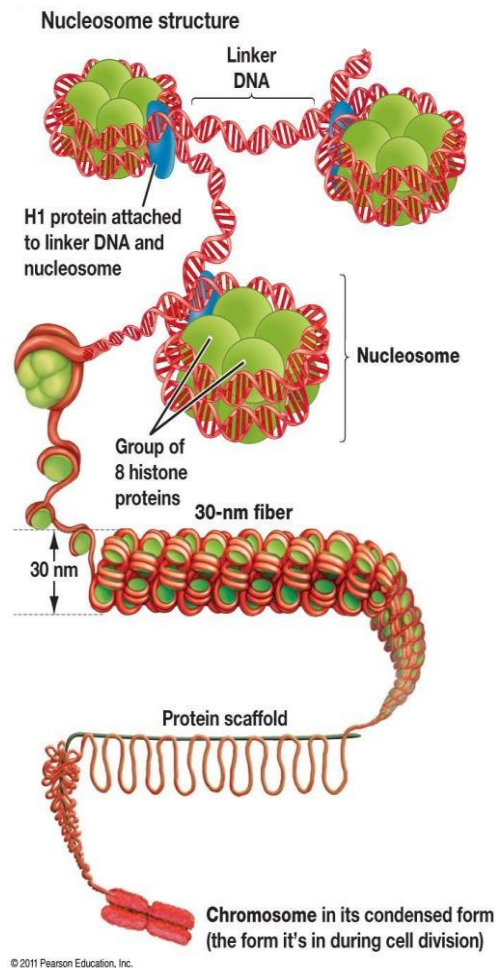


Figure 1.2 : (a) Complex structure (Ferenc et al., 2013) (b) Forming aggregate (Ainalem and Nylanderet, 2011)

In cell nucleus DNA is wrapped around positively charged protein known as histone and forms the nucleosome structure, these nucleosomes form higher order structure like beads on a string and produce chromatin structure (Kornberg and Lorch, 1999) (see Figure 1.3).



Electrostatic complexation of the negatively charged DNA chains with polyvalent cations is the primary mechanism for DNA compaction in gene therapy field (Evans et al., 2003), for improving and development of efficient gene transfer into eukaryotic cells (transfection efficiency) (Dennig and Duncan, 2002).

Some theoretical models have been proposed to provide further understanding of the structure of DNA chains/polyvalent cations like Mateescu's model and Schiessel's model. (Mateescu et al., 1999; Schiessel et al., 2001)

Figure 1.3: Nucleosome structure (Image reproduced from Pearson Education ,Inc.)

1.4 Previous studies

Qamhieh and coworkers applied a theoretical model developed by H. Schiessel, who considered complexes of positively charged hard spheres and a persistent linear polyelectrolyte. They provided further understanding of the formation and the structure of

Dendrimer/DNA complexes by studying the effect of dendrimer size on the optimal length of the DNA chain adsorbed by the dendrimer, Then Qamhieh and Khaleel developed a model for Sphere/DNA complex similar to the one developed by H.Schiessel, but with ion-penetrable sphere (soft sphere) instead of hard sphere (ion-impenetrable) to make it more realistic to express the dendrimer/DNA complex(Qamhieh et al., 2009; Qamhieh and Khaleel, 2013). The effect of size, charge density of the dendrimer, and other factors on the structure of the complex were studied and compared with data predicted previously by analytical study done by Qamhieh for G_2 , G_4 , G_6 , and G_8 of PAMAM dendrimers-DNA complexations (Qamhieh and Khaleel, 2013). One of The first studies about interactions between colloidal particles was published in 1991. Both Ducker (Ducker et al., 1991) and Butt have replaced the normal force-sensing tip with a small glass sphere, to obtain the first experimental measurements of the interaction between a colloidal particle and a glass or mica surface (Ducker et al., 1991) (Butt, 1991). Then in 1993 the interactions forces versus distance between pairs of 2 μm diameter polystyrene spheres immersed in electrolytes containing up to 1 M KCl were measured (Li et al., 1993), then thousands of studies were done after which related to the interactions between two small colloidal particles.

Recently, nanoparticle–cell interaction has become increasingly important for improving our current understanding of how various nanoparticles, like some drug substances, interact with cells, including the interaction during three stages: before penetration, during penetration (uptaking), and after cell-membrane-penetrating (engulfed) stage. There are many factors that affect the nanoparticle–cell interaction, namely, size, shape, net, and type of the charge surfaces of particles (substances) and other factors associated with the interaction's medium, have been studied during the last few years (Verma and Stellacci, 2009; Lee and Larson, 2009).

1.5 Theoretical model (Three stage model):

Ohshima derived a model for the electrostatic interaction between two soft spheres (penetrable spheres) embedded in a neutral salt solution in three stages as in Figure (2.1) (Ohshima, 2013).

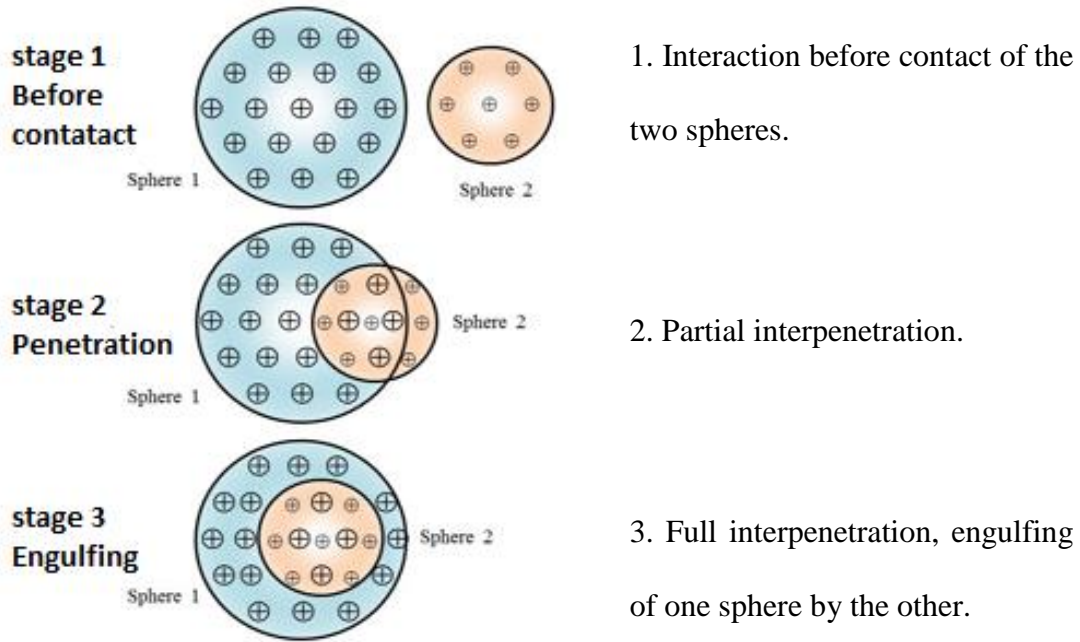


Figure 1.4: The three stages of interaction between two soft charged spheres

Analytic expressions for the electrostatic interaction between two interpenetrating weakly charged spherical soft particles (space-charged porous spheres) in an electrolyte solution was driven on the basis of the linearized Poisson-Boltzmann equation for the electric potential distribution (Ohshima, 2013).

1.5.1 Electrostatic interactions between soft particles:

Electrostatic interactions between soft particles are quite different from those for hard particles without surface structures in that the electrostatic interactions between soft particles are governed by their space-charges distributed within the particles or the Donnan potentials, while those for hard particle are determined by their surface charges or

potentials. Theoretical studies on the interaction between soft particles have so far been confined mostly to the interactions before contact of the surface layers of the interacting particles (Ohshima, 2008).

1.5.2 Linearized Poisson-Boltzmann equations for two interacting charged porous spheres (soft spheres):

Consider two charged porous spheres of radii a_1 and a_2 carrying fixed charges of Constant volume densities ρ_1 and ρ_2 , respectively, at separation R between their centers O_1 and O_2 in an electrolyte solution containing N ionic species with valence z_i and bulk concentration (number density) n_i ($i = 1, 2 \dots N$) (in units of m^{-3}) in three stages, that is,

(i) interaction before contact, (ii) interpenetration, and (iii) engulfing (see Figure 1.4) .

If dissociated groups of valence Z_j are distributed at a uniform density N_j in sphere j ($j = 1, 2$), then the fixed-charge density ρ_j in sphere j is related to the density N_j by $\rho_j = Z_j e N_j$ ($j=1, 2$). Without loss of generality, we may treat the case in which the radius a_1 of sphere 1 is larger than or equal to the radius a_2 of sphere 2,

$$a_1 \geq a_2 \quad (1)$$

Ohshima assumed that the relative permittivity in spheres 1 and 2 take the same value ϵ_r as that of the electrolyte solution and that the electrical potential Ψ is low enough to allow the linearization of the Poisson-Boltzmann equations for Ψ .

The linearized Poisson-Boltzmann equation in the respective regions can generally

be given by:

$$\Delta\Psi = \kappa^2\Psi - \frac{\rho}{\epsilon_r\epsilon_0} \quad (2)$$

$$\text{With } \kappa = \left(\frac{1}{\epsilon_r \epsilon_0 kT} \sum_{i=1}^N z_i^2 e^2 n_i \right)^{1/2} \quad (3)$$

Where κ is the Debye-Hückel parameter (Dähnert and Rödenbeck, 1994), and $(1/\kappa)$ is the Debye length, measure of a charge carrier's net electrostatic effect in solution, and how far those electrostatic effects persist, depends on n the bulk concentration and z the valence of ions.

By using eq. 3 Expression for a symmetrical electrolyte (like NaCl solution) of valence z and bulk concentration n is given by:

$$\kappa = \left(\frac{2z^2 e^2 n}{\epsilon_r \epsilon_0 kT} \right)^{1/2}$$

$z=1$ for monovalent solution, $z=2$ for divalent, and for trivalent $z=3$

The fixed-charge density ρ in the respective regions in the three stages is shown in following:

Stage 1:

Interaction before contact

$$\rho = \begin{cases} \rho_1 & \text{for region I} \\ \rho_2 & \text{for region II} \\ 0 & \text{for region III} \end{cases} \quad (4)$$

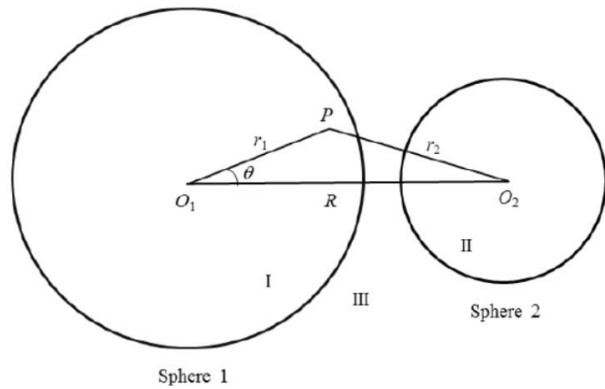


fig. 1.5a

Stage 2: Interpenetration

$$\rho = \begin{cases} \rho_1 & \text{for region I} \\ \rho_2 & \text{for region II} \\ \rho_1 + \rho_2 & \text{for region III} \\ 0 & \text{for region IV} \end{cases} \quad (5)$$

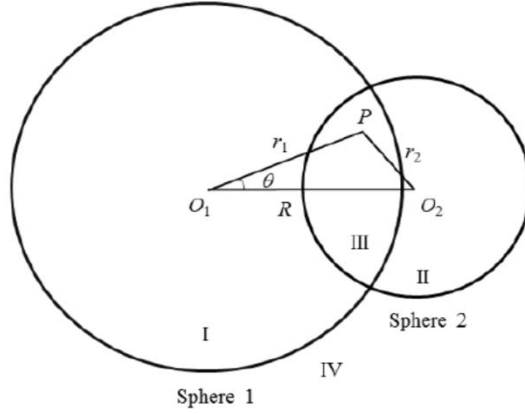


fig.1.5b

Stage 3 : Engulfing

$$\rho = \begin{cases} \rho_1 & \text{for region I} \\ \rho_1 + \rho_2 & \text{for region II} \\ 0 & \text{for region III} \end{cases} \quad (6)$$

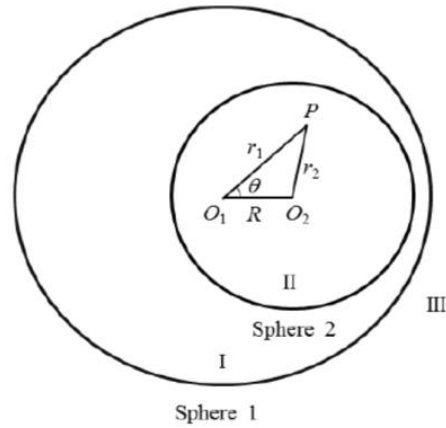


fig.1.5c

Figure 1.5 : The fixed-charge density ρ in the respective regions in the three stages (a) Stage 1

(b) Stage 2 (c) Stage 3

The boundary conditions are :

$$1) \Psi \rightarrow 0 \text{ at points far from spheres 1 and 2} \quad (7)$$

$$2) \Psi \text{ and } (d\Psi/dn) \text{ are continuous at the surfaces of spheres 1 and 2} \quad (8)$$

The derivative of Ψ being taken along the outward normal to the surface of each sphere.

The solution to Eq. (2) can be expressed as the sum

$$\Psi = \Psi_1 + \Psi_2 \quad (9)$$

Where Ψ_1 and Ψ_2 are, respectively, the unperturbed potentials for spheres 1 and 2 in the absence of the interaction between the two spheres.

This is because of:

(i) Eq. (2) is linear with respect to Ψ and (ii) when the boundary conditions at the sphere surface are given by Eq. (6), the unperturbed potential of one sphere automatically satisfies the boundary conditions at the surface of the other sphere.

The potential distribution Ψ for the system of two interacting ion-penetrable spheres are thus simply given by linear superposition of the unperturbed potentials Ψ_1 and Ψ_2 produced by the respective spheres.

Thus one needs to solve only the potential distribution for a single isolated sphere.

Consider the unperturbed potential Ψ_1 produced by sphere 1, for which Eq (2) reduces to

$$\frac{d^2\Psi_{1out}}{dr_1^2} + \frac{2}{r} \frac{d\Psi_{1out}}{dr_1} = \kappa^2\Psi_{1out} \text{ for } r_1 > a_1 \text{ (outside sphere 1)} \quad (10)$$

$$\frac{d^2\Psi_{1in}}{dr_1^2} + \frac{2}{r} \frac{d\Psi_{1in}}{dr_1} = \kappa^2\Psi_{1in} - \frac{\rho_1}{\epsilon_r\epsilon_0} \text{ for } 0 \leq r < a_1 \text{ (inside sphere 1)} \quad (11)$$

$$\Psi_{1out}(r_1) \rightarrow 0 \text{ as } r_1 \rightarrow \infty \quad (12)$$

$$\Psi_{1in}(a_1^-) = \Psi_{1out}(a_1^+) \quad (13)$$

$$\left. \frac{d\Psi_{1in}}{dr_1} \right|_{r_1=a_1^-} = \left. \frac{d\Psi_{1out}}{dr_1} \right|_{r_1=a_1^+} \quad (14)$$

Where r_1 is the distance measured from the center O_1 of sphere 1.

The solutions to Eqs. (10) and (11) subject to Eqs. (12)-(14) are:

$$\Psi_1(r_1) = \begin{cases} \Psi_{1out}(r_1) & \text{for } r_1 \geq a_1 \text{ (outside sphere 1)} \\ \Psi_{1in}(r_1) & \text{for } 0 \leq r_1 \leq a_1 \text{ (inside sphere 1)} \end{cases} \quad (15)$$

Where

$$\Psi_{1out}(r_1) = \frac{\rho_1}{\varepsilon_r \varepsilon_0 \kappa^2} \left\{ \cosh(\kappa a_1) - \frac{\sinh(\kappa a_1)}{\kappa a_1} \right\} a_1 \frac{e^{-\kappa r_1}}{r_1} \quad (16)$$

$$\text{and } \Psi_{1in}(r_1) = \frac{\rho_1}{\varepsilon_r \varepsilon_0 \kappa^2} \left\{ 1 - \left[1 + \frac{1}{\kappa a_1} \right] a_1 e^{-\kappa a_1} \frac{\sinh(\kappa r_1)}{\kappa r_1} \right\} \quad (17)$$

Similarly, Ohshima derived the potential Ψ_2 produced by sphere 2 in the absence of sphere 1, which Ψ_2 is obtained by replacing r_1 with r_2 and a_1 with a_2 in Eqs. (15)-(17). The result is:

$$\Psi_2(r_2) = \begin{cases} \Psi_{2out}(r_2) & \text{for } r_2 \geq a_2 \text{ (outside sphere 2)} \\ \Psi_{2in}(r_2) & \text{for } 0 \leq r_2 \leq a_2 \text{ (inside sphere 2)} \end{cases} \quad (18)$$

Where:

$$\Psi_{2out}(r_2) = \frac{\rho_2}{\varepsilon_r \varepsilon_0 \kappa^2} \left\{ \cosh(\kappa a_2) - \frac{\sinh(\kappa a_2)}{\kappa a_2} \right\} a_2 \frac{e^{-\kappa r_2}}{r_2} \quad (19)$$

$$\Psi_{2in}(r_2) = \frac{\rho_2}{\varepsilon_r \varepsilon_0 \kappa^2} \left\{ 1 - \left[1 + \frac{1}{\kappa a_2} \right] a_2 e^{-\kappa a_2} \frac{\sinh(\kappa r_2)}{\kappa r_2} \right\} \quad (20)$$

where r_2 is the radial coordinate measured from the center $O2$ of sphere 2, which is related to r_1

$$r_2 = (R^2 + r_1^2 - 2Rr_1 \cos \theta)^{1/2} \quad (21)$$

The prefactors of Eqs. (16), (17), (19), and (20) are equal to the Donnan Potentials Ψ_{DON1} and Ψ_{DON2} in spheres 1 and 2, respectively. (Ohshima, 2010)

$$\Psi_{DONi} = \frac{\rho_i}{\varepsilon_r \varepsilon_0 \kappa^2} \quad (i = 1, 2) \quad (22)$$

1.5.2.1 Stage 1: Interaction between two porous spheres before contact

Consider two spheres 1 and 2 of radii a_1 and a_2 at separation R before their contact with each other, i.e., $R \geq a_1 + a_2$. In this stage there are three regions I (inside sphere 1 and outside sphere 2), II (outside sphere 1 and inside sphere 2), and III (outside both spheres 1 and 2) (see Figure 2.2a). Note that the fixed charge densities in the respective regions are ρ_1 for region I, ρ_2 for region II, and zero for region III (Eq. (4)). The potentials in the respective regions are given by

$$\Psi = \begin{cases} \Psi_{1in}(r_1) + \Psi_{2out}(r_2) & \text{for region I} \\ \Psi_{1out}(r_1) + \Psi_{2in}(r_2) & \text{for region II} \\ \Psi_{1out}(r_1) + \Psi_{2out}(r_2) & \text{for region III} \end{cases} \quad (23)$$

The interaction energy $V^*(R)$ between two charged porous spheres 1 and 2 at separation R can be obtained from the free energy $F(R)$ of the system of two spheres 1 and 2 minus that at infinite separation ($R \rightarrow \infty$), viz., $V^*(R) = F(R) - F(\infty)$. Here $F(R)$ in stage 1 is given by

$$F(R) = \frac{1}{2} \rho_1 \int_{V_I} \Psi dV_I + \frac{1}{2} \rho_2 \int_{V_{II}} \Psi dV_{II} \quad (24)$$

Where integration is carried out over the volumes V_I and V_{II} of the respective regions I and II, and $F(\infty)$ is given by

$$F(\infty) = \frac{1}{2} \rho_1 \int_{V_I} \Psi_{1in} dV_I + \frac{1}{2} \rho_2 \int_{V_{II}} \Psi_{2in} dV_{II} \quad (25)$$

which is the sum of the electrostatic self-free energies of spheres 1 and 2.

$$V^*(R) = F(R) - F(\infty) = \frac{1}{2}\rho_1 \int_{V_I} \Psi_{2out} dV_I + \frac{1}{2}\rho_2 \int_{V_{II}} \Psi_{1out} dV_{II} \quad (26)$$

By substituting Eq. (16) and (19) into Eq. (26), Ohshima obtained after some algebra

$$V^*(R) = \frac{4\pi a_1 a_2 \rho_1 \rho_2}{\varepsilon_r \varepsilon_0 \kappa^4} \left\{ \cosh(\kappa a_1) - \frac{\sinh(\kappa a_1)}{\kappa a_1} \right\} \left\{ \cosh(\kappa a_2) - \frac{\sinh(\kappa a_2)}{\kappa a_2} \right\} \frac{e^{-\kappa R}}{R}$$

(27)

for $R \geq a_1 + a_2$

The interaction force $P^*(R) = -dV^*(R)/dR$ is then given by

$$P^*(R) = \frac{4\pi a_1 a_2 \rho_1 \rho_2}{\varepsilon_r \varepsilon_0 \kappa^4} \left\{ \cosh(\kappa a_1) - \frac{\sinh(\kappa a_1)}{\kappa a_1} \right\} \left\{ \cosh(\kappa a_2) - \frac{\sinh(\kappa a_2)}{\kappa a_2} \right\} \frac{(\kappa R + 1)e^{-\kappa R}}{R^2}$$

(28)

for $R \geq a_1 + a_2$

1.5.2.2 Stage 2: Interaction between two partially interpenetrating charged porous spheres

Consider two partially interpenetrating spheres 1 and 2 of radii a_1 and a_2 at Separation R ($a_1 - a_2 < R < a_1 + a_2$). In this stage there are three regions I (inside sphere 1 and outside sphere 2), II (outside sphere 1 and inside sphere 2), III (inside both spheres 1 and 2), and IV (outside both spheres 1 and 2) (see Figure 2.2b). Note that the fixed charge densities in the respective regions are ρ_1 for region I, ρ_2 for region II, $\rho_1 + \rho_2$ for region III, and zero for region IV.

The potentials in the respective regions are given by:

$$\Psi = \begin{cases} \Psi_{1in}(r_1) + \Psi_{2out}(r_2) & \text{for region I} \\ \Psi_{1out}(r_1) + \Psi_{2in}(r_2) & \text{for region II} \\ \Psi_{1in}(r_1) + \Psi_{2in}(r_2) & \text{for region III} \\ \Psi_{1out}(r_1) + \Psi_{2out}(r_2) & \text{for region IV} \end{cases} \quad (29)$$

The free energy $F(R)$ of the system of two spheres 1 and 2 in stage 2 is given by

$$F(R) = \frac{1}{2}\rho_1 \int_{V_I} \Psi dV_I + \frac{1}{2}\rho_2 \int_{V_{II}} \Psi dV_{II} + \frac{1}{2}(\rho_1 + \rho_2) \int_{V_{III}} \Psi dV_{III} \quad (30)$$

Thus the interaction energy $V^*(R)$ between two charged porous spheres 1 and 2 at separation R in stage 2 is

$$\begin{aligned} V^*(R) &= F(R) - F(\infty) \\ &= \frac{1}{2}\rho_1 \int_{V_I} \Psi_{2out} dV_I + \frac{1}{2}\rho_2 \int_{V_{II}} \Psi_{1out} dV_{II} + \frac{1}{2}\rho_1 \int_{V_{III}} \Psi_{2in} dV_{III} + \frac{1}{2}\rho_2 \int_{V_{III}} \Psi_{1in} dV_{III} \\ &\text{for } (a_1 - a_2 < R < a_1 + a_2). \end{aligned} \quad (31)$$

By substituting Eqs. (16), (17), (19) and (20) into Eq. (31), Ohshima obtained after some algebra

$$\begin{aligned} V^*(R) &= \frac{4\pi a_1 a_2 \rho_1 \rho_2}{\epsilon_r \epsilon_0 \kappa^4 R} \left[\frac{1}{\kappa^2 a_1 a_2} \left\{ 1 + \frac{\kappa^2}{2} (R^2 - a_1^2 - a_2^2) \right\} + \frac{\kappa^2}{24 a_1 a_2} (R - a_1 - a_2)^2 \{ R^2 + \right. \\ &2(a_1 + a_2)R - 3(a_1 - a_2)^2 \} + \left[1 - \frac{1}{\kappa^2 a_1 a_2} \right] e^{-\kappa R} \cosh(\kappa(a_1 - a_2)) - \left[\frac{1}{\kappa a_1} - \right. \\ &\left. \left. \frac{1}{\kappa a_2} \right] e^{-\kappa R} \sinh(\kappa(a_1 - a_2)) - \left[1 + \frac{1}{\kappa a_1} \right] \left[1 + \frac{1}{\kappa a_2} \right] e^{-\kappa(a_1 + a_2)} \sinh(\kappa R) \right] \end{aligned}$$

$$\text{For } a_1 - a_2 \leq R \leq a_1 + a_2 \quad (32)$$

The interaction force $P^*(R) = -dV^*(R)/dR$ is then given by

$$P^*(R) = \frac{4\pi a_1 a_2 \rho_1 \rho_2}{\epsilon_r \epsilon_0 \kappa^4 R^2} \left[\left[1 + \frac{1}{\kappa a_1} \right] \left[1 + \frac{1}{\kappa a_2} \right] \{ (\kappa R + 1)e^{-\kappa(R+a_1+a_2)} + (\kappa R - 1)e^{-\kappa(R-a_1-a_2)} \} + \right. \\ \left. \left[1 + \frac{1}{\kappa a_1} \right] \left[1 - \frac{1}{\kappa a_2} \right] (\kappa R + 1)e^{-\kappa(R+a_1-a_2)} + \left[1 - \frac{1}{\kappa a_1} \right] \left[1 + \frac{1}{\kappa a_2} \right] (\kappa R + 1)e^{-\kappa(R-a_1+a_2)} + \right. \\ \left. \kappa^2 a_1 a_2 \left[1 - \frac{1}{(\kappa a_1)^2} \right] \left[1 - \frac{1}{(\kappa a_2)^2} \right] - \frac{1}{\kappa^2 a_1 a_2} \{ (\kappa R)^2 - 1 \} - \frac{\kappa^2}{4a_1 a_2} (R^2 - a_1^2 - a_2^2)^2 \right]$$

$$\text{For } a_1 - a_2 \leq R \leq a_1 + a_2 \quad (33)$$

1.5.2.3 Stage 3: Interaction for the case where sphere 2 is engulfed by sphere 1

Consider two spheres 1 and 2 of radii a_1 and a_2 at separation R for the case in which $0 \leq R \leq a_1 - a_2$ so that sphere 2 is engulfed by sphere 1. In this stage there are three regions I (inside sphere 1 and outside sphere 2), II (inside spheres 1 and 2), and III (outside spheres 1 and 2) (see Figure 2.2c).

Note that the fixed charge densities in the respective regions are ρ_1 for region I, $\rho_1 + \rho_2$ for region II, and zero for region III. The potentials in the respective regions are given by

$$\Psi = \begin{cases} \Psi_{1in}(r_1) + \Psi_{2out}(r_2) & \text{for region I} \\ \Psi_{1in}(r_1) + \Psi_{2in}(r_2) & \text{for region II} \\ \Psi_{1out}(r_1) + \Psi_{2out}(r_2) & \text{for region III} \end{cases} \quad (34)$$

The free energy $F(R)$ of the system of two spheres 1 and 2 in stage 3 is given by

$$F(R) = \frac{1}{2} \rho_1 \int_{V_I} \Psi dV_I + \frac{1}{2} (\rho_1 + \rho_2) \int_{V_{II}} \Psi dV_{II} \quad (35)$$

Thus the interaction energy $V^*(R)$ between two charged porous spheres 1 and 2 at separation R in stage 3 is

$$V^*(R) = F(R) - F(\infty)$$

$$= \frac{1}{2}\rho_1 \int_{V_I} \Psi_{2out} dV_I + \frac{1}{2}\rho_1 \int_{V_{II}} \Psi_{2in} dV_{II} + \frac{1}{2}\rho_2 \int_{V_{II}} \Psi_{1in} dV_{II} \quad (36)$$

By substituting Eqs. (17), (19) and (20) into Eq. (34), Ohshima obtained after some algebra

$$V^*(R) = \frac{4\pi a_1 a_2 \rho_1 \rho_2}{\varepsilon_r \varepsilon_0 \kappa^4 R} \left[\frac{(\kappa a_2)^2 R}{3a_1} - \left[1 + \frac{1}{\kappa a_1} \right] e^{-\kappa a_1} \left\{ \cosh(\kappa a_2) - \frac{\sinh(\kappa a_2)}{\kappa a_2} \right\} \sinh(\kappa R) \right]$$

for $0 \leq R \leq a_1 - a_2$ (37)

The interaction force $P^*(R) = -dV^*(R)/dR$ is then given by

$$P^*(R) = \frac{4\pi a_1 a_2 \rho_1 \rho_2}{\varepsilon_r \varepsilon_0 \kappa^4 R^2} \left[\{(\kappa R) \cosh(\kappa R) - \sinh(\kappa R)\} \left[1 + \frac{1}{\kappa a_1} \right] e^{-\kappa a_1} \left\{ \cosh(\kappa a_2) - \frac{\sinh(\kappa a_2)}{\kappa a_2} \right\} \right]$$

for $0 \leq R \leq a_1 - a_2$ (38)

(Ohshima, 2013;2010).

The three-stage model of the electrostatic interaction between two charged interpenetrating charged spherical soft particles without the particle core in an electrolyte solution is presented by H.Ohshima . That is, (i) interaction before contact of the two spheres, (ii) partial interpenetration, and (iii) full interpenetration, i.e., engulfing of one sphere by the other. H.Ohshima derived the interaction energies and forces for the respective stages on the basis of the linearized Poisson-Boltzmann equations for the electric potential distribution. (Ohshima, 2013)

1.6 Statement of the problem:

The aim is to understand the nature of the interaction between complexes (DNA/dendrimer) and other soft particles (such as cells) in introducing the genetic material into cells, which is still a great challenge in gene therapy.

We used the three-stage model derived by Ohshima (Ohshima, 2013). By applying this model we obtained some mathematical functions that supply us with valuable information about important parameters' affect on the electrostatic interaction between soft charged particles. As an example, we obtained functions that describe the effect on the maximum electrostatic interaction force behavior by varying certain parameters, namely, charge, size, permittivity, temperature and concentration of the salt solution.

Throughout this analytical study, these functions give us an ability to control the conditions of the interaction to get the most desired transfection efficiency in gene therapy.

Chapter Two

The Model and Method

Chapter Two

2.1 Introduction

The electrostatic interactions between small (nano particles) soft charged particles were studied by using the three-stage model that describes the electrostatic interaction between two soft charged spheres through three stages (Ohshima, 2013). The following equations have been taken and simplified to be suitable for applying to this model.

2.2 Electrostatic interaction energy and force before the penetration

The electrostatic interaction energy between two soft charged spheres before the penetration is

$$V^*(R) = \frac{4\pi a_1 a_2 \rho_1 \rho_2}{\epsilon_r \epsilon_0 \kappa^4} \left\{ \cosh(\kappa a_1) - \frac{\sinh(\kappa a_1)}{\kappa a_1} \right\} \left\{ \cosh(\kappa a_2) - \frac{\sinh(\kappa a_2)}{\kappa a_2} \right\} \frac{e^{-\kappa R}}{R} \quad (2.1)$$

The electrostatic interaction force between two soft charged spheres before the penetration is

$$P^*(R) = \frac{4\pi a_1 a_2 \rho_1 \rho_2}{\epsilon_r \epsilon_0 \kappa^4} \left\{ \cosh(\kappa a_1) - \frac{\sinh(\kappa a_1)}{\kappa a_1} \right\} \left\{ \cosh(\kappa a_2) - \frac{\sinh(\kappa a_2)}{\kappa a_2} \right\} \frac{(\kappa R + 1)e^{-\kappa R}}{R^2} \quad (2.2)$$

(Ohshima, 2013)

2.3 Electrostatic interaction energy and force during the penetration

The electrostatic interaction energy between two soft charged spheres during the penetration is given by

$$\begin{aligned} V^*(R) = & \frac{4\pi a_1 a_2 \rho_1 \rho_2}{\epsilon_r \epsilon_0 \kappa^4 R} \left[\frac{1}{\kappa^2 a_1 a_2} \left\{ 1 + \frac{\kappa^2}{2} (R^2 - a_1^2 - a_2^2) \right\} + \frac{\kappa^2}{24 a_1 a_2} (R - a_1 - a_2)^2 \{ R^2 + \right. \\ & 2(a_1 + a_2)R - 3(a_1 - a_2)^2 \} + \left[1 - \frac{1}{\kappa^2 a_1 a_2} \right] e^{-\kappa R} \cosh(\kappa(a_1 - a_2)) - \left[\frac{1}{\kappa a_1} - \right. \\ & \left. \left. \frac{1}{\kappa a_2} \right] e^{-\kappa R} \sinh(\kappa(a_1 - a_2)) - \left[1 + \frac{1}{\kappa a_1} \right] \left[1 + \frac{1}{\kappa a_2} \right] e^{-\kappa(a_1 + a_2)} \sinh(\kappa R) \right] \quad (2.3) \end{aligned}$$

The electrostatic interaction force between two soft charged spheres during the penetration

$$P^*(R) = \frac{4\pi a_1 a_2 \rho_1 \rho_2}{\varepsilon_r \varepsilon_0 \kappa^4 R^2} \left[\left[1 + \frac{1}{\kappa a_1} \right] \left[1 + \frac{1}{\kappa a_2} \right] \{ (\kappa R + 1) e^{-\kappa(R+a_1+a_2)} + (\kappa R - 1) e^{-\kappa(R-a_1-a_2)} \} + \right. \\ \left. \left[1 + \frac{1}{\kappa a_1} \right] \left[1 - \frac{1}{\kappa a_2} \right] (\kappa R + 1) e^{-\kappa(R+a_1-a_2)} + \left[1 - \frac{1}{\kappa a_1} \right] \left[1 + \frac{1}{\kappa a_2} \right] (\kappa R - 1) e^{-\kappa(R-a_1+a_2)} + \right. \\ \left. \kappa^2 a_1 a_2 \left[1 - \frac{1}{(\kappa a_1)^2} \right] \left[1 - \frac{1}{(\kappa a_2)^2} \right] - \frac{1}{\kappa^2 a_1 a_2} \{ (\kappa R)^2 - 1 \} - \frac{\kappa^2}{4 a_1 a_2} (R^2 - a_1^2 - a_2^2)^2 \right] \quad (2.4)$$

(Ohshima, 2013)

2.4 Electrostatic interaction energy and force after the penetration

The electrostatic interaction energy between two soft charged spheres after the penetration is given by:

$$V^*(R) = \frac{4\pi a_1 a_2 \rho_1 \rho_2}{\varepsilon_r \varepsilon_0 \kappa^4 R} \left[\frac{(\kappa a_2)^2 R}{3 a_1} - \left[1 + \frac{1}{\kappa a_1} \right] e^{-\kappa a_1} \left\{ \cosh(\kappa a_2) - \frac{\sinh(\kappa a_2)}{\kappa a_2} \right\} \sinh(\kappa R) \right] \quad (2.5)$$

The electrostatic interaction force between two soft charged spheres after the penetration

$$P^*(R) = \frac{4\pi a_1 a_2 \rho_1 \rho_2}{\varepsilon_r \varepsilon_0 \kappa^4 R^2} \left[\{ (\kappa R) \cosh(\kappa R) - \sinh(\kappa R) \} \left[1 + \frac{1}{\kappa a_1} \right] e^{-\kappa a_1} \left\{ \cosh(\kappa a_2) - \frac{\sinh(\kappa a_2)}{\kappa a_2} \right\} \right] \quad (2.6) \quad (\text{Ohshima, 2013})$$

2.5 Simplification:

For simplifying the electrostatic interaction energies and forces equations, we can write the prefactor (A) of interaction energy and force equations as in the following form :

$$A = \frac{4\pi a_1 a_2 \rho_1 \rho_2}{\varepsilon_r \varepsilon_0 \kappa^4 R^2} = \frac{4\pi a_1 a_2}{\varepsilon_r \varepsilon_0 \kappa^4 R^2} \left(\frac{3Q_1}{4\pi a_1^3} \right) \left(\frac{3Q_2}{4\pi a_2^3} \right) \quad (2.7)$$

where $Q_j = e Z_j$ is the net charge on sphere j, and Z_j is the number charge

by substituting Q_1 and Q_2 we thus obtain :

$$A = \frac{9e^2 Z_1 Z_2}{\epsilon_r \epsilon_0 \kappa^4 R^2 (4\pi a_1^2 a_2^2)} \quad (2.8)$$

By multiplying with $(\frac{k_B T}{k_B T})$, we can get :

$$A = \frac{9 Z_1 Z_2 l_B}{\kappa^4 R^2 a_1^2 a_2^2} (k_B T) \quad (2.9)$$

Where l_B is the Bjerrum length $l_B = e^2 / 4\pi \epsilon_r \epsilon_0 k_B T$ (2.10)

The Bjerrum length is the separation distance in nm unit at which the electrostatic interaction between two elementary charges is comparable in magnitude to the thermal energy scale $k_B T$, where k_B is Boltzmann constant and T is the absolute temperature in Kelvin (Messina et al., 2013).

Bjerrum length is equal to 0.7nm at room temperature $T \approx 300$ K, where the dielectric constant of water $\epsilon_r = 80$.

By using the last form of the Prefactor A and the interaction equations of $V^*(R)$ we can get :

$$V(R) = V^*(R) / k_B T, \quad \text{Where } V(R) \text{ is the interaction energy in units of } k_B T.$$

Here, by applying the equations of interaction energies and forces with the new prefactor (A), The electrostatic interactions between a dendrimer and a cell could be calculated and studied.

Chapter Three

Results and Discussions

Chapter Three

Results and Discussions

3.1 Introduction :

We are studying the electrostatic interaction between two penetrable spheres according to a model derived by Ohshima, to understand the effect of some factors on the behavior of the interaction under certain conditions through three stages of the interaction: before penetration stage (equations 2.1 and 2.2), during penetration stage (equations 2.3 and 2.4) and after penetration (engulfed) stage (equations 2.5 and 2.6).

3.2 Effect of some parameters on interaction between two soft spheres

The focus in this case of our study has been on charge number Z , sizes of particles, permittivity, temperature, concentration of the salt solution, and valence z of ions parameters. The interactions are affected by those as shown in the following sections:

3.2.1 Effect of the particle's charge on the electrostatic interaction:

By using Ohshima's model we have calculated the interaction energies and forces between two soft spheres with constant radii $a_1 = 10$ nm and $a_2 = 5$ nm, with the charge number of sphere 1 fixed at $Z_1 = 100$, while on the other hand, sphere 2 takes different values of charge numbers Z_2 (1, 10, 20, 50, and 100). The interactions were studied and calculated at room temperature into monovalent 10mM salt solution, which corresponds to Debye screening length of 3nm and Bjerrum length of 0.71nm (see Figure 3.1).

The measured interaction energies increase by increasing Z_2 , with the highest calculated interaction being at $Z_2 = 100$ and the lowest at $Z_2 = 1$ (an almost neutral particle has a

charge of an electron e) as shown in Figure 3.1. The charge volume density of the last particle ($Z_2 = 1$), is very small compared with others. It is clear that the interaction heavily depends on the charge number Z , and this may explain the strength of interaction of polymers that have high branches, large Z , and high charge densities with other charged particles and charged surfaces. As in many polyelectrolyte (PE) adsorption experiments, the highly charged PEs adsorb strongly to oppositely charged interfaces. This affinity is primarily caused by attractive and repulsive electrostatic forces acting between the charged PE and substrate (Szilagyi et al., 2014).

Along the penetration region where $5 < R < 15$ corresponding to $(a_1 - a_2 < R < a_1 + a_2)$, which is bounded by the vertical lines as shown in Figure (3.1), the interactions show active changes for all cases. During this interval, the energies increase more rapidly than in the other stages of interaction, the interaction forces increase to a certain point (the maximum point) and then decrease.

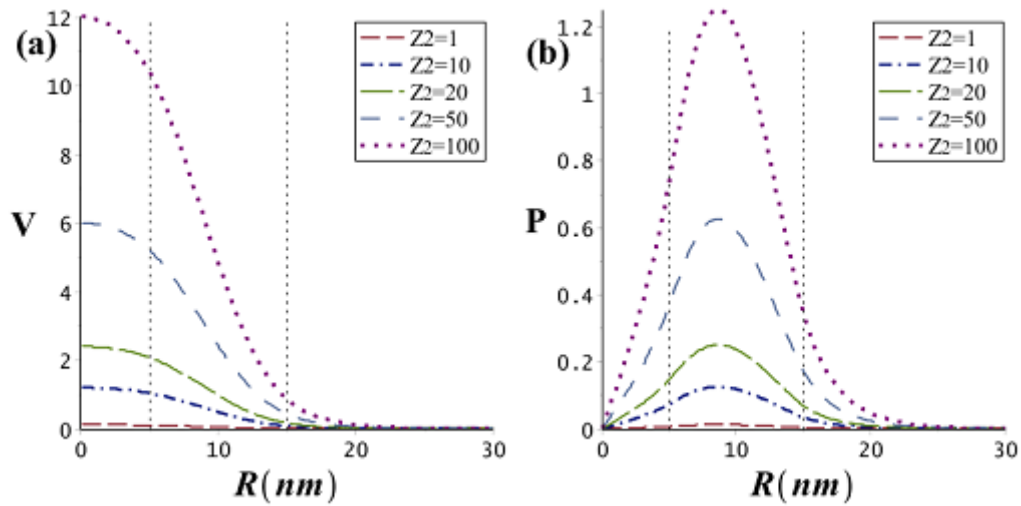


Figure 3.1: Interactions measurements between soft sphere1 ($a_1=10\text{nm}$, $Z_1=100$), and soft sphere2 ($a_2=5\text{nm}$) where $Z_2 = 1, 10, 20, 50$ and 100 for each case (a) Interaction energy V as a function of distance R (b) The interaction force as a function of distance R for each case of (a)

The distance R_{max} , where the maximum force occurs, was determined for all cases by derivation ($\frac{dP}{dR} = 0$). We found that no effect of the charge number Z was observed. In other words, all maximum force points occur at the same distance ($R_{max} = 8.63$ nm) for all interaction force curves, independent of charge number Z , as in Figure (3.2).

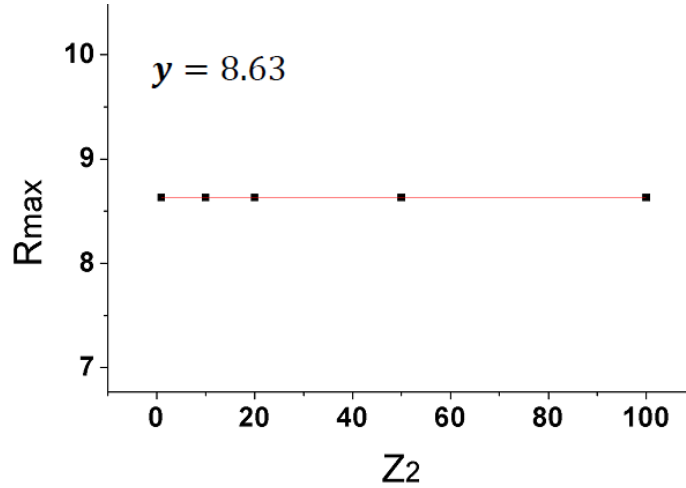


Figure 3.2: R_{max} in nm unit versus Z , where R_{max} is distance R at the maximum interaction force value P_{max}

3.2.2 Size effect on the electrostatic interaction between two soft charged spheres:

Here, we summarize the impact of size on interactions between soft nano particles. The interaction energies and forces of soft sphere with radius $a_1=10$ nm, and five soft particles with different radii ($a_2=1$ nm, 4nm, 6nm, 8nm, and 10 nm) are immersed into monovalent 10mM salt solution, at room temperature, were calculated and compared as shown in Figure (3.3). Charge number of all particles was fixed at same value $Z=10$, hence, the interaction increases with decreasing a_2 (see Figure 3.4a) during stages 2 and 3 but decreases during stage 1. The increasing can be explained by increasing the volume charge density which depending on a_2 while Z takes fixed value for all particles in this

section, in other words the highest energy related to the particle has the highest volume charge density. The interaction forces curves being sharp with increasing a_2 (see Figure 3.3b).

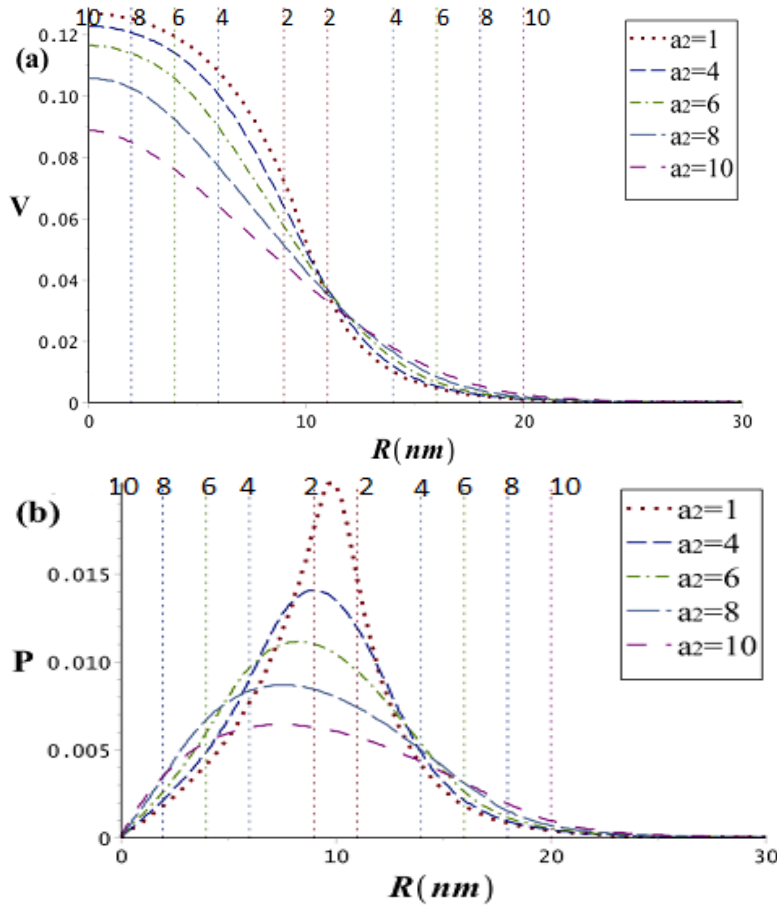


Figure 3.3: (a) Interaction energy where $a_1=10$ nm and $a_2=1$ nm, 4 nm, 6 nm, 8 nm, 10 nm, in all cases $Z_1=Z_2=10$, $l_B=0.7$ nm, and the salt concentration = 10 mM (b) The interaction force versus distance R for each case

The shifts of the maximum force locations during the full penetration intervals ($2 a_2$) were observed and determined. The ratio (B) between the shift of R_{max} from the lower limit ($10 - a_2$) of the penetration region, bounded by $a_1 - a_2$ and $a_1 + a_2$ (as shown by vertical lines), and the interval between the upper and the lower limits (always equal to $2 a_2$) was calculated, as shown in table (3.1), and plotted versus the radius of sphere 2 (a_2) as in Figure (3.4b). Here, the y-intercept represents the location of the maximum point on the

penetration interval, in other words, the maximum force always occurs during the second third of penetration interval .

Table 3.1: The ratio B represents the location of the maximum force point [$R_{max} - (a_1 - a_2)$] to the length of penetration interval ($2 a_2$), where a_1, a_2 are radii of sphere 1 and sphere2 respectively.

$B=[R_{max} - (a_1 - a_2)]/2 a_2$	0.310	0.358	0.347	0.350	0.355
$a_2(\text{nm})$	1	4	6	8	10

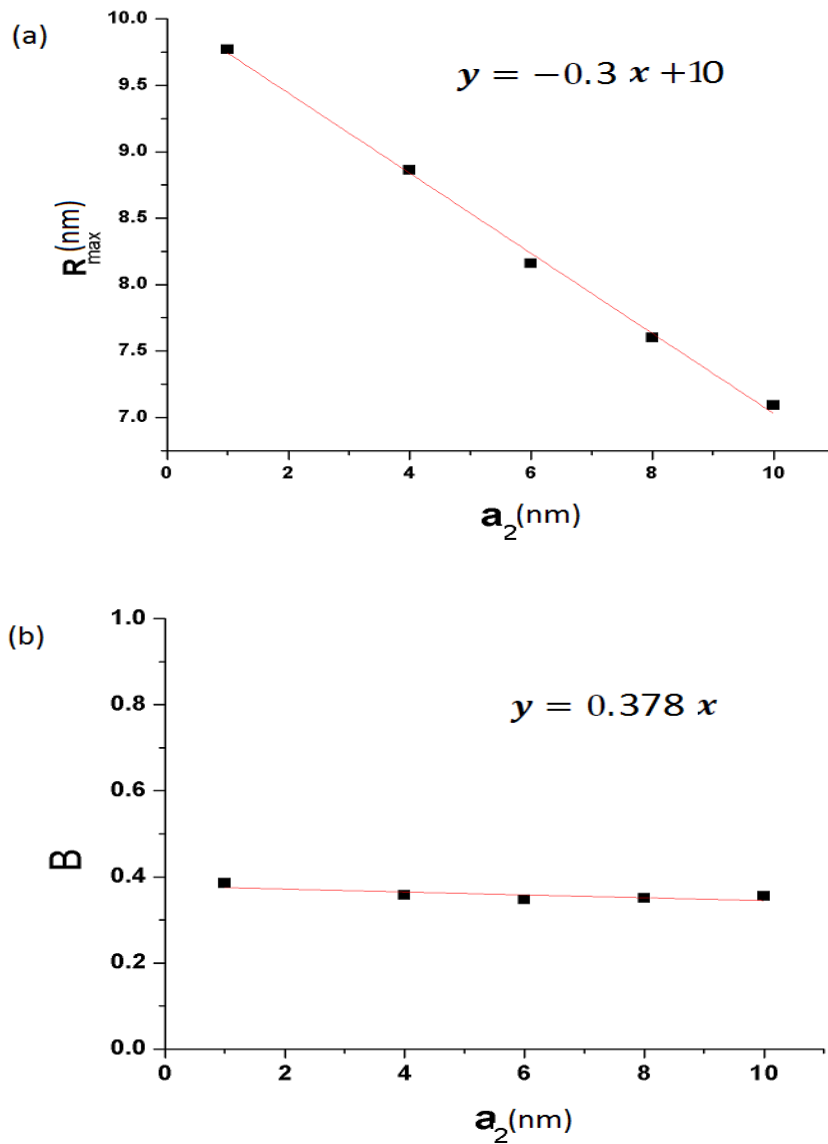


Figure 3.4: (a) The distance R at the maximum interaction force versus a_2 in nm unit. (b) The ratio B [distance of R_{max} from lower term of penetration interval ($a_1 - a_2$) to length of penetration interval ($2 a_2$), which is bounded by upper term ($a_1 + a_2$) and lower term ($a_1 - a_2$)], versus the radius of sphere 2 in nm.

3.2.3.1 Effect of monovalent salt concentration measured by inverse Debye length (κ):

The effect of the salt concentration on the interaction between two soft spheres that are immersed in salt solution has been studied. We selected two main cases to study this effect on the interaction. Namely, the first case is the interaction of G_2 , G_4 , G_6 , and G_8 of PAMAM dendrimer and a charged sphere in nano scale has a radius equal to 10 nm, and the second case the interaction with a charged sphere in micro scale (1 micro radius). The two cases were included in our study because there are several scientific studies in the fields of gene therapy and drug delivery that are related with PAMAM dendrimers' interactions with particles in micro scale, like silica particles, biological cells, and particles in nano scale like protein and gold nanoparticles. The particles could be soft like cells and proteins, and hard like silica and gold particles, depending on the degree of penetration.

In this part of our study, Bjerrum length (l_B) corresponds to 0.7 nm at room temperature, the calculations have been performed for interactions in an aqueous solution. The interaction energy of each case has been calculated, and it seemed to increase as the salt concentration decreased (Debye screening length becomes larger) as it shown in figures (3.5, 3.8). In stage 1 (before the interpenetration) at separation $R > (10+R_g)$ for Case 1, and $R > (1000+R_g)$ for Case 2, where R_g is the radius of generation of dendrimer G_n , n is an integer number refers to the order of the generation, at the whole of this separation the interactions show the same behavior in each case of the large and small sphere. (See figures (3.5), (3.8)).

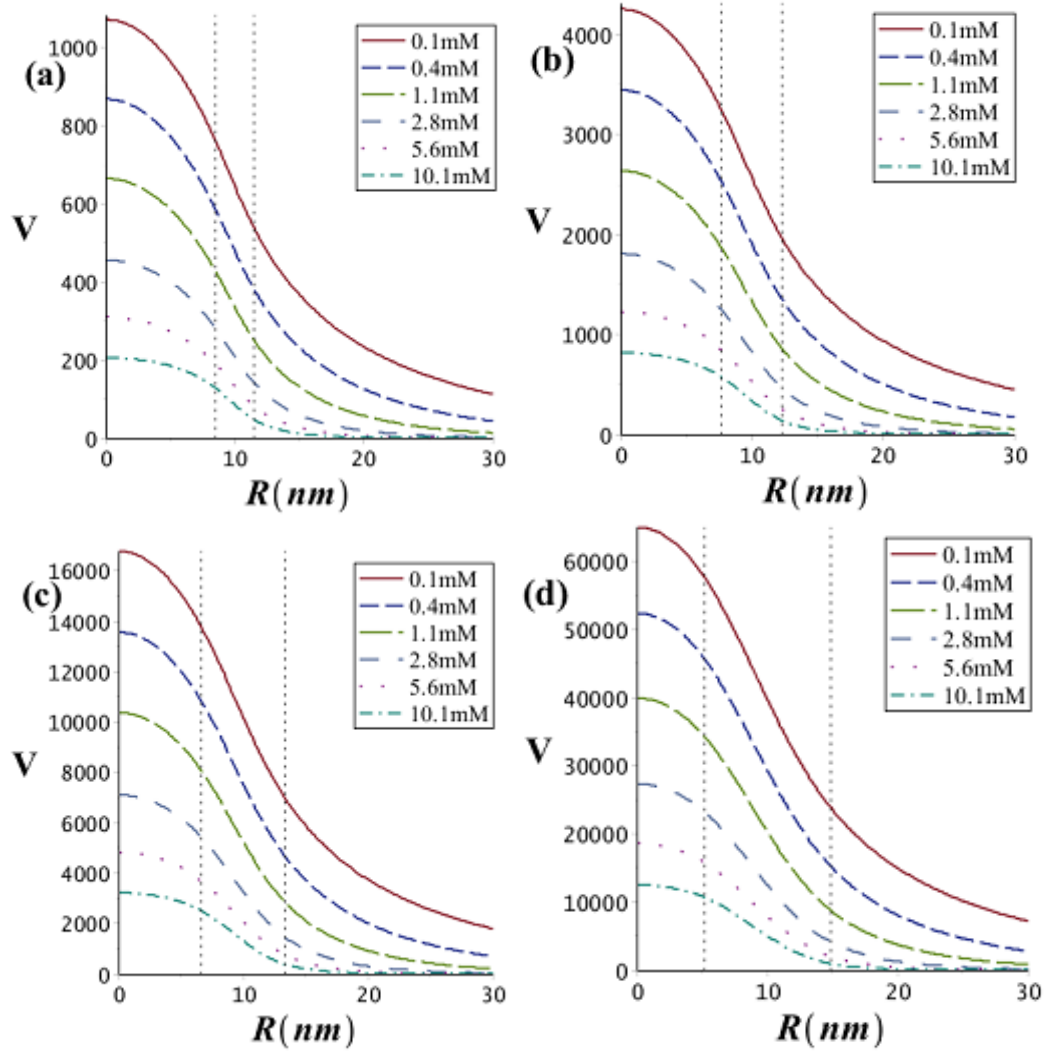


Figure 3.5: The interaction energy $V(R)$ of a sphere with radius $a=10\text{nm}$ and $Z=10,000$ immersed in monovalent aqueous solution ($l_B=0.7$) takes different concentration values 0.1, 0.4, 1.1, 2.8, 5.6, 10.1mM interacts with (a) G_2 (b) G_4 (c) G_6 (d) G_8 .

After penetration interval ($R < 10 - R_g$) in Case 1, which is bounded by vertical lines, the interaction force decreases to the minimum value almost linearly for low concentration values (see Figure 3.6) while the force during the third region ($R < 1000 - R_g$) in Case 2 decreases exponentially and rapidly as we increase the concentration (see Figure 3.9).

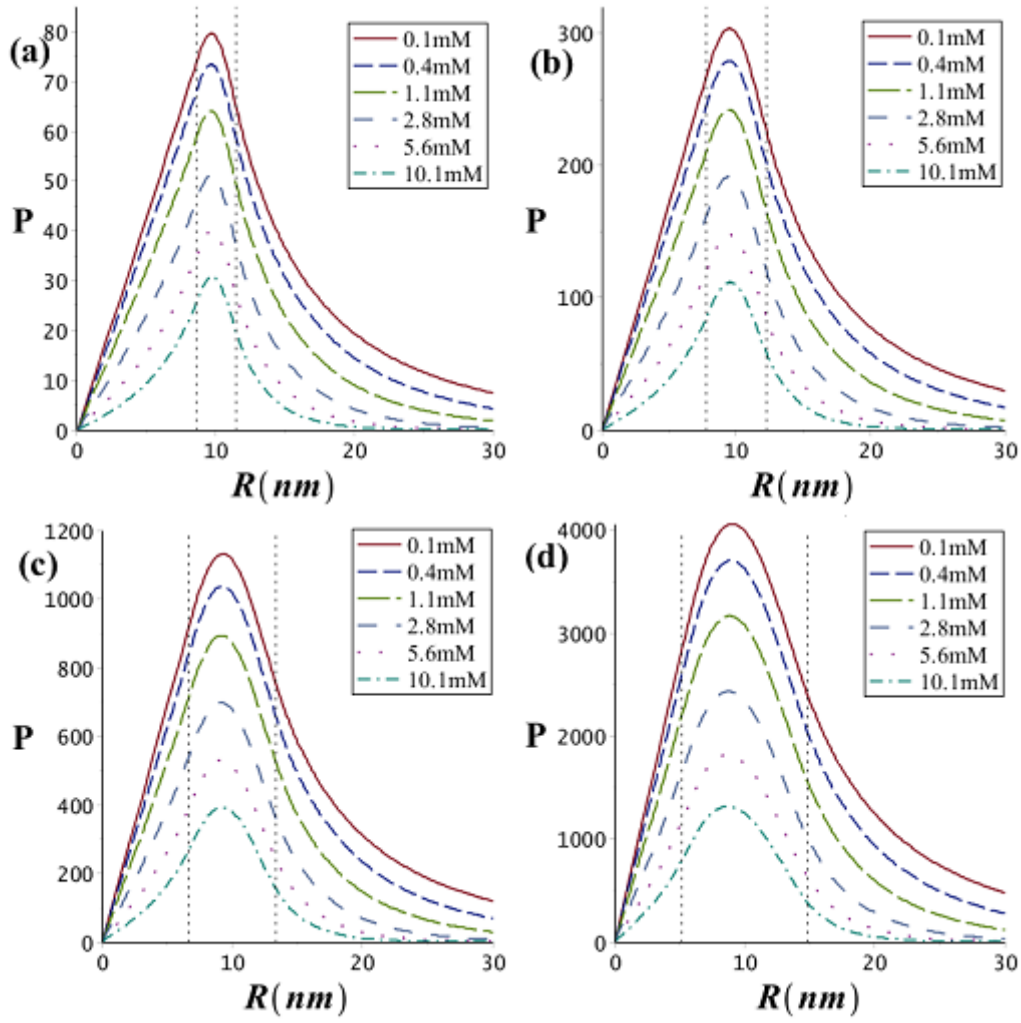


Figure 3.6: The interaction force $P(R)$ of a sphere with radius $a=10\text{nm}$ and $Z=10,000$ immersed in monovalent aqueous solution ($l_B=0.7$) takes concentration values 0.1 , 0.4, 1.1, 2.8, 5.6, 10.1mM interacts with (a) G_2 (b) G_4 (c) G_6 (d) G_8 .

Here, we focused on the interaction force between some generations of PAMAM dendrimer and the nano and micro soft spheres, we can see from figure (3.6), during the stages of interaction, It is clear that the shape of all these curves is unsymmetrical and the interaction force changed more rapidly in the first stage side (before contact), that could be explained by the screening effect of the solution's ions. the maximum force values behavior with varying the concentration has been studied, for Case 1 (nano sphere)

the interaction force changes by the relation $(m + dx^c)^{-1}$ (see Figure 3.7), while the interaction force in Case 2 (micro sphere) is shown to be changed by the relation ax^{-b} (see Figure 3.10), where, a, b, c, d, and m are factors related to the generation G_n of dendrimer. From Figures (3.7, 3.10) we can see the magnitudes of m and d factors decrease while c factor increases with increasing number n (the order of generation G_n), on the other hand, a and b factors increase with increasing n .

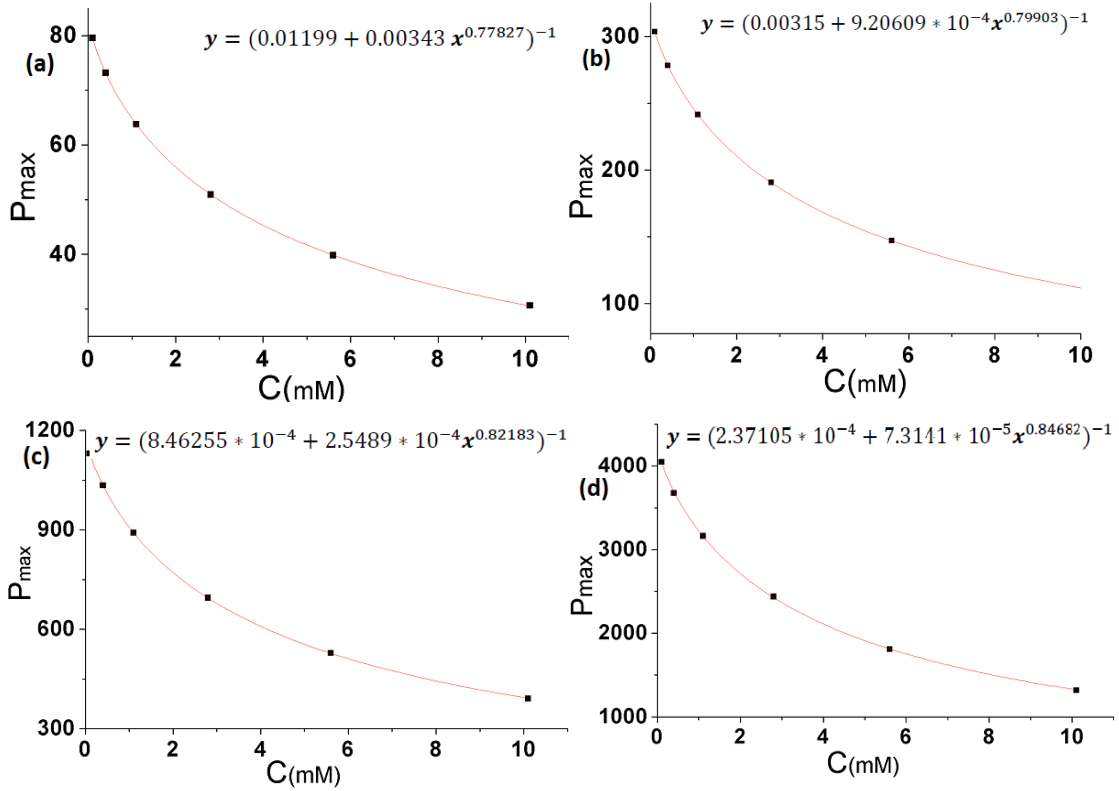


Figure 3.7: The maximum interaction force P_{max} versus Concentration C in mM unit when a sphere with 10nm radius and number Charge $Z=10,000$ interacts with (a) G_2 (b) G_4 (c) G_6 (d) G_8 .

Here, the gaps between the interaction energies and forces are increased clearly in Case 2 compared with Case 1, as shown in figures (3.8), (3.9).

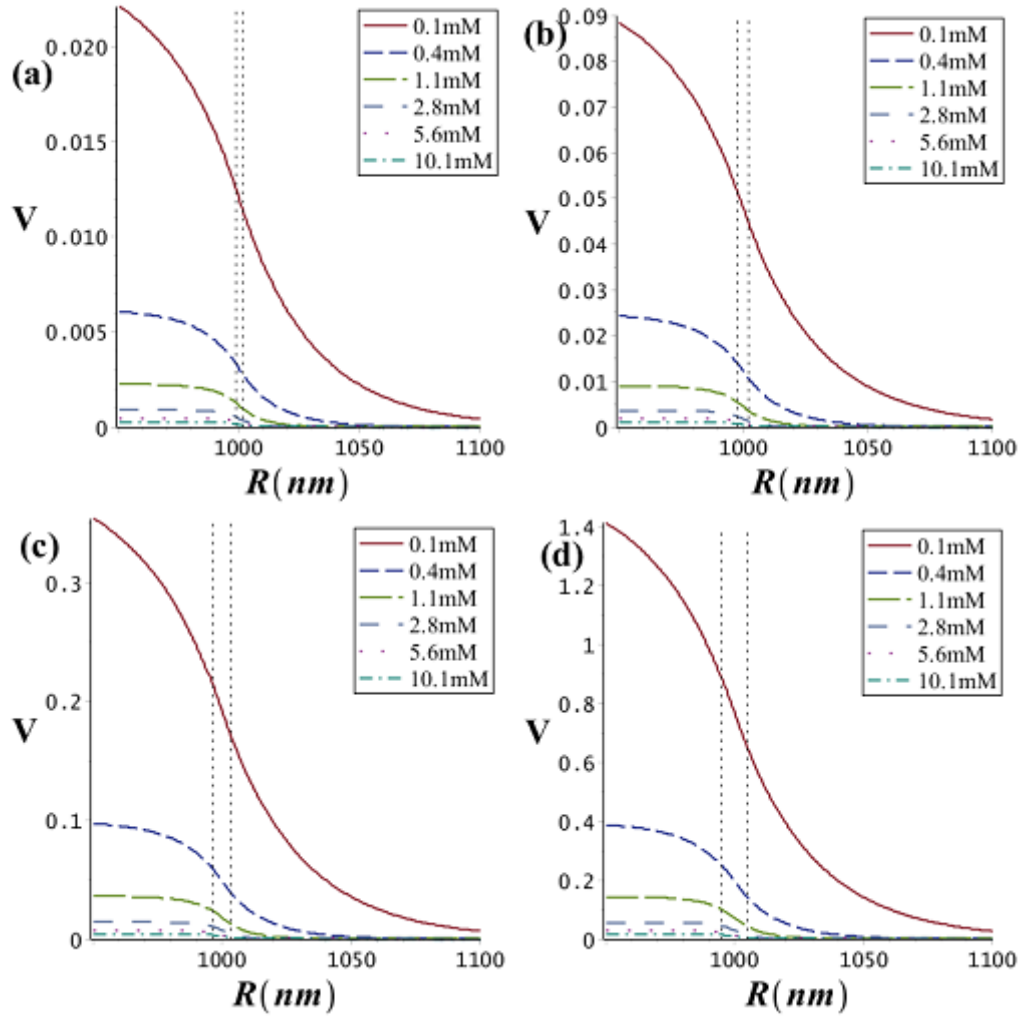


Figure 3.8: The interaction energy $V(R)$ of a sphere with radius $a=1,000\text{nm}$ and $Z=10,000$ immersed in a monovalent aqueous solution ($l_B=0.7$) with concentration values of 0.1, 0.4, 1.1, 2.8, 5.6, 10.1mM interacting with (a) G_2 (b) G_4 (c) G_6 (d) G_8 .

In this case the interaction force curves being symmetrical, sharp, and sharper with G_2, G_4 (see Figure 3.9), in other words, the behavior of interaction forces before and after penetration seemed to be reflected during the short penetration interval that could be

explained by the following, the sphere's charge density responds to the close proximity of the second charged sphere (G_n) by becoming displaced away from the point of contact but after contact the structure of inside the sphere makes screening of electrostatic force's effect seems like the screening effect of the ions outside (before contact) the interpenetrating particles (a charged sphere with radius $a = 1,000\text{nm}$ and G_n). (Stace and Bichoutskaia, 2012)

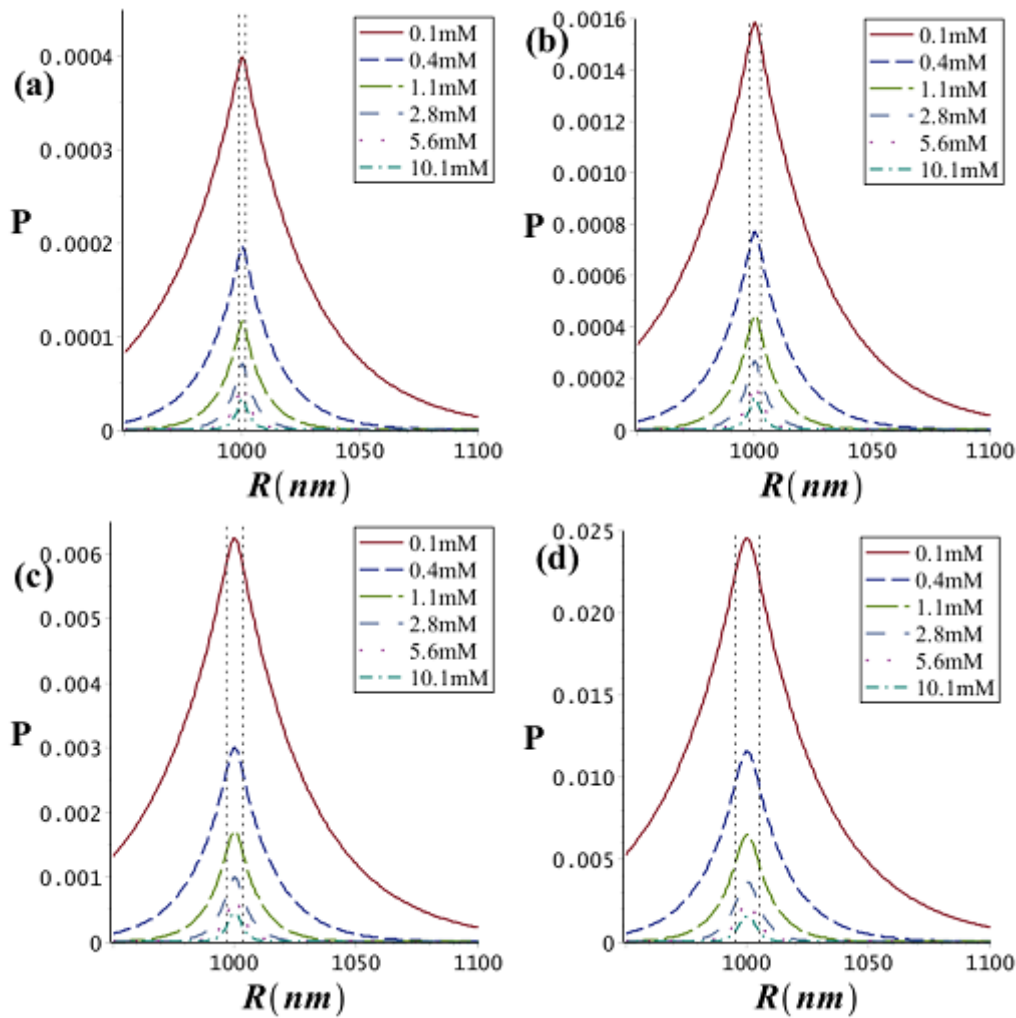


Figure 3.9: The interaction force $P(R)$ of a sphere with radius $a = 1,000\text{nm}$ and $Z=10,000$ immersed in a monovalent aqueous solution ($l_B=0.7$) taking concentration values 0.1, 0.4, 1.1, 2.8, 5.6, 10.1mM interacts with (a) G_2 (b) G_4 (c) G_6 (d) G_8 .

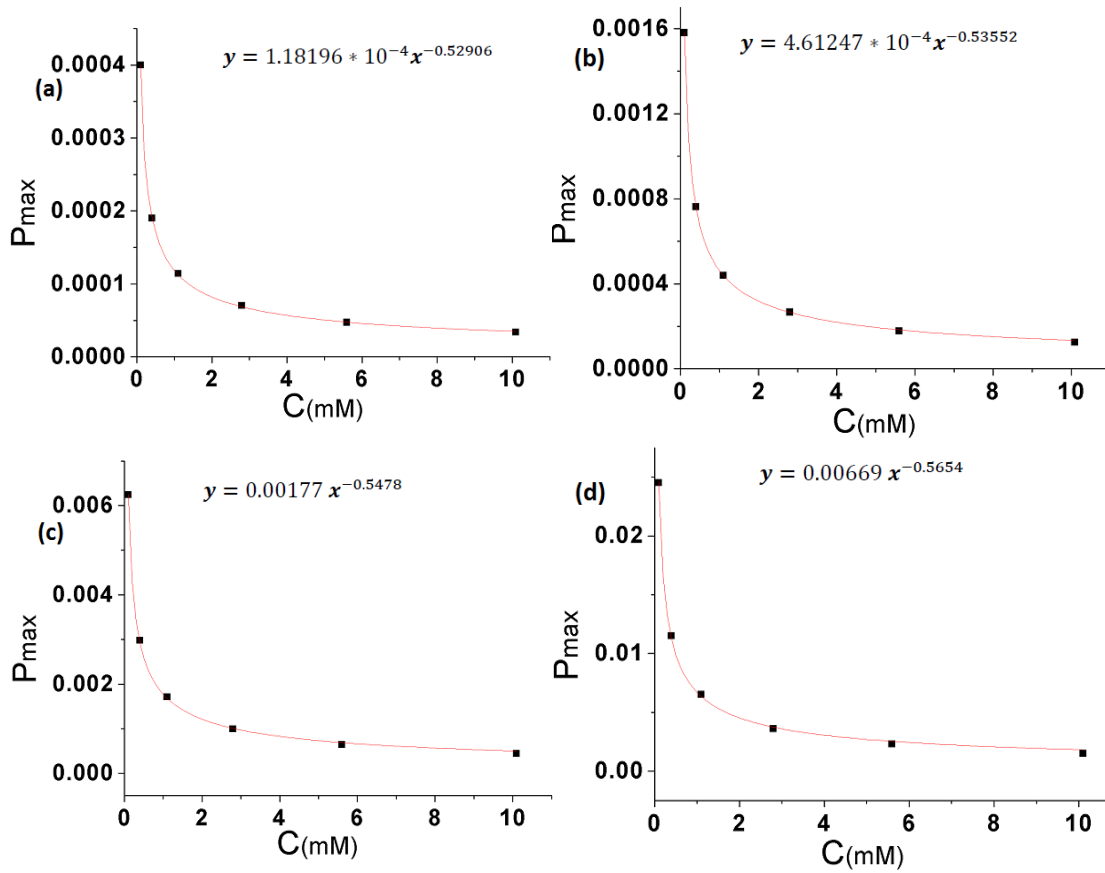


Figure 3.10: The maximum interaction force P_{max} versus Concentration C in mM unit when a sphere with 1,000nm radius and charge number $Z=10,000$ interacts with (a) G_2 (b) G_4 (c) G_6 (d) G_8 .

3.2.3.2 Effect of ion's valence of the salt on the interaction between two soft interpenetrating charged spheres:

The interaction energies and forces between a soft sphere with 10 nm radius and generations G_2 , G_4 , G_6 , and G_8 of PAMAM dendrimers, are immersed in a solution with 10.1 mM salt concentration, are calculated for monovalent ($z=1$), divalent ($z=2$) and trivalent ($z=3$) salt.

Figure (3.11) shows that the interaction energy in all cases decreases by increasing z , the highest interactions related to monovalent salt solution. For divalent and trivalent cases the

interaction energies is slightly changed during the third stage $R < (10 - R_g)$, especially with G_2 and G_4 , (where R_g is the radius of generation of PAMAM dendrimer) (see table 1.1). The ratio of interaction energy of G_n to the interaction energy of G_{n+2} is found around 0.25, where $n = 2, 4, 6$.

In the divalent and trivalent cases curves are closer to each other than the monovalent one (see Figure 3.11).

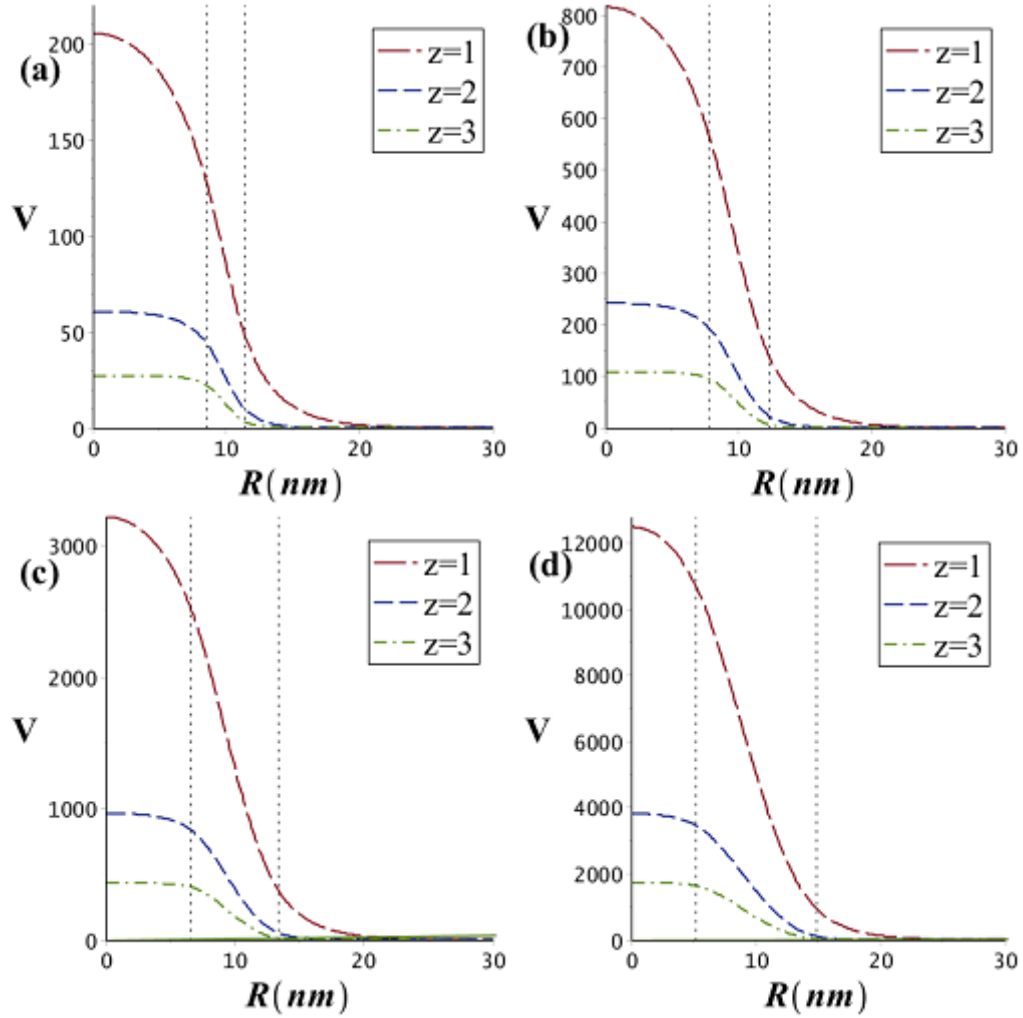


Figure 3.11: Interaction energy of a sphere with 10nm radius and $Z=10,000$ immersed in three solutions, the solutions have the same salt concentration 10mM and $l_B=0.7$ but various values of valence of ions in each solution $z = 1, 2, 3$ interacting with (a) G_2 (b) G_4 (c) G_6 (d) G_8 .

The interaction force curves become sharper and more symmetric with decreasing n of the generation. The maximum force occurs during the second third of the penetration interval. For monovalent case with G_8 the interaction force along the curve in the third interval $R < (10 - R_g)$ shows linearly behavior (see Figure 3.12).

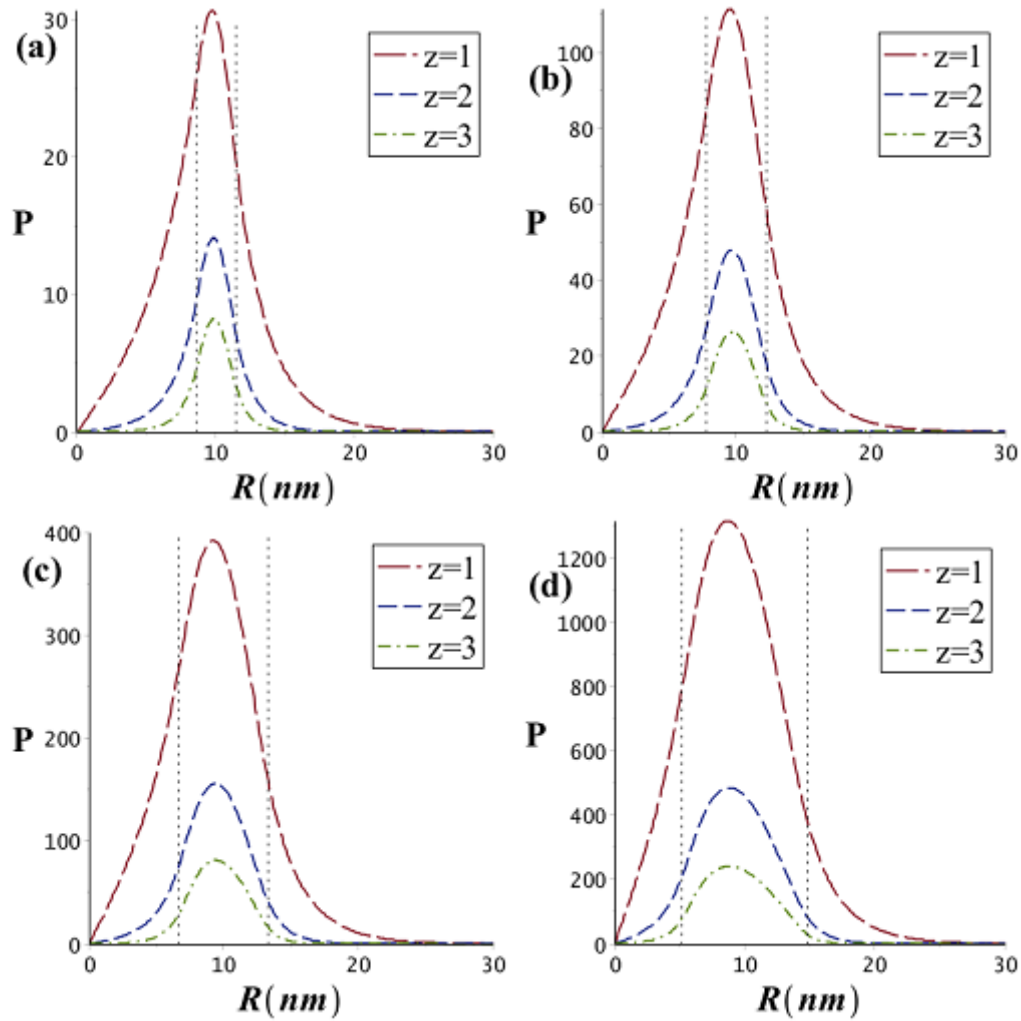


Figure 3.12: Interaction force of a sphere with 10nm radius and $Z=10,000$ immersed in three solutions; having the same salt concentration 10mM and $l_B=0.7$ but various values of valence ions in each solution $z = 1, 2, 3$ interacting with (a) G_2 (b) G_4 (c) G_6 (d) G_8 .

3.2.4 Effect of Bjerrum length l_B on the interaction:

We first performed different sets of calculations, including varying salt concentration with fixed Bjerrum length l_B as in the last section. We now turn to varying the Bjerrum length while fixing the other parameters, which affects the interactions. Two effects included in l_B were studied, namely, the relative permittivity ϵ_r and the temperature T in Kelvin.

3.2.4.1 Effect of Relative permittivity ϵ_r on the interactions under fixed temperature:

As in the salt concentration effect section for studying the interactions with varying l_B , similarly, we have taken two main cases of interactions, the interaction energies and forces for a system consists of one sphere of nano scale radius contacts with the generations G_2, G_4, G_6, G_8 , and another system consists of a sphere in micro scale with charge number Z equals to 10,000 with the same generations under same certain conditions .

The interaction energies and forces for the two systems in a monovalent aqueous solution with fixed concentration at value $C=10\text{mM}$ were calculated and studied with varying relative permittivity in range (62,93) which closes to the range of permittivity of water. Table (3.2) shows the l_B values correspond to some selected relative permittivity values at room temperature in Kelvin (298 K).

We can see from figures (3.13), (3.14) that the interactions change slightly during the first stage of interaction; $R > (10 - R_g)$ in Case1 and $R > (1000 - R_g)$ in Case2, compared with the rest of interaction's intervals (during and after penetration). In general, the interaction increases by increasing Bjerrum length l_B as shown in figures (3.13), (3.14), (3.16), (3.17).

Table 3.2 : The measured values of l_B in nm unit correspond to some selected ϵ_r values at room temperature.

ϵ_r	93	86	80	75	70	66	62
l_B (nm)	0.6	0.65	0.7	0.75	0.8	0.85	0.9

We have observed that the interval of the penetration increases by increasing order (n) of generation (G_n), in other words, the length of penetration interval depends on radius of generation R_g .

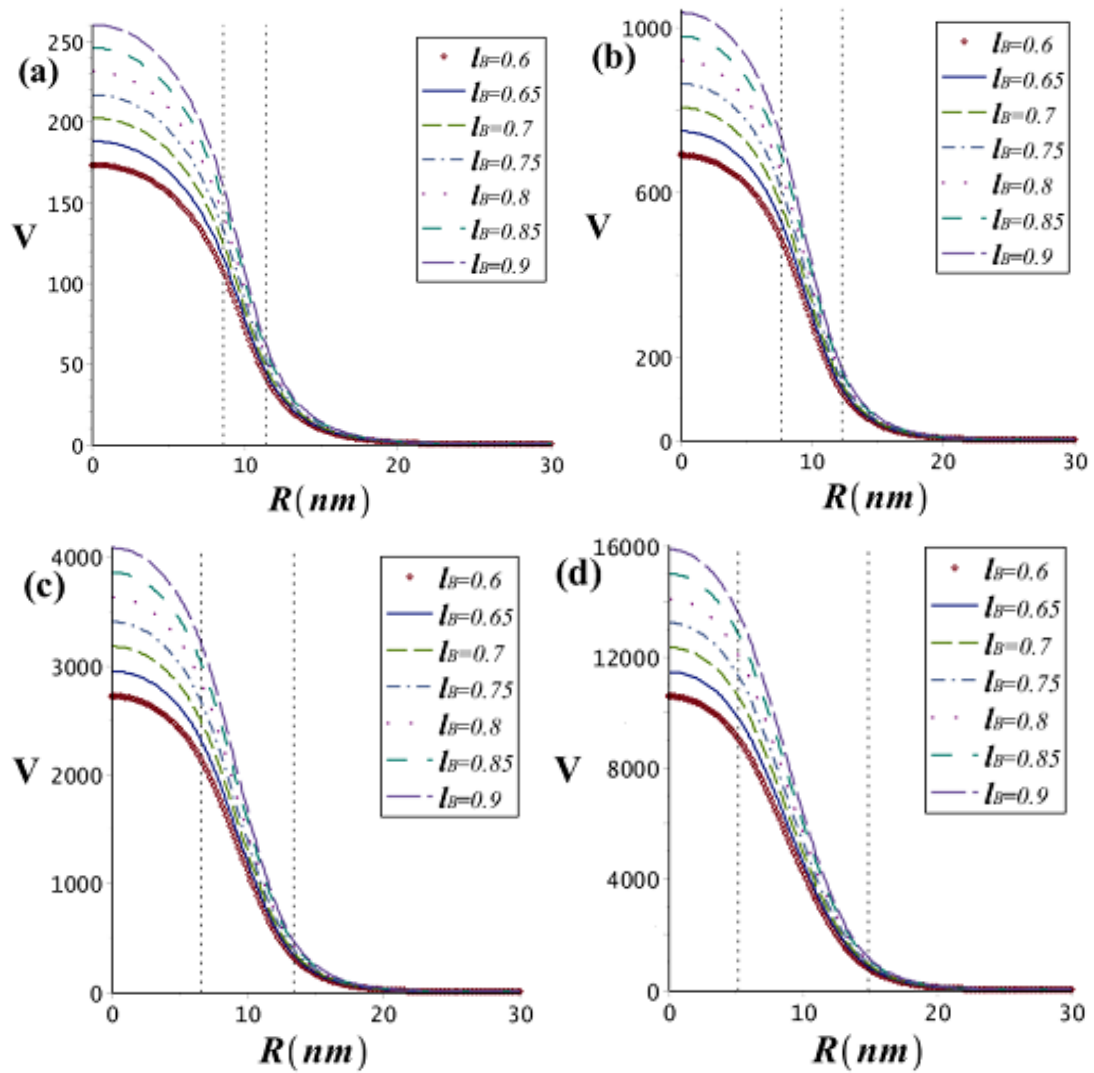


Figure 3.13: The interaction energy $V(R)$ of a sphere with radius $a = 10$ nm and $Z = 10000$ immersed in an Monovalent aqueous solution with 10 mM concentration and Bjerrum length takes different values $l_B = 0.6, 0.65, 0.7, 0.75, 0.8, 0.85, 0.9$ nm in each case at room temperature interacts with (a) G_2 (b) G_4 (c) G_6 (d) G_8 .

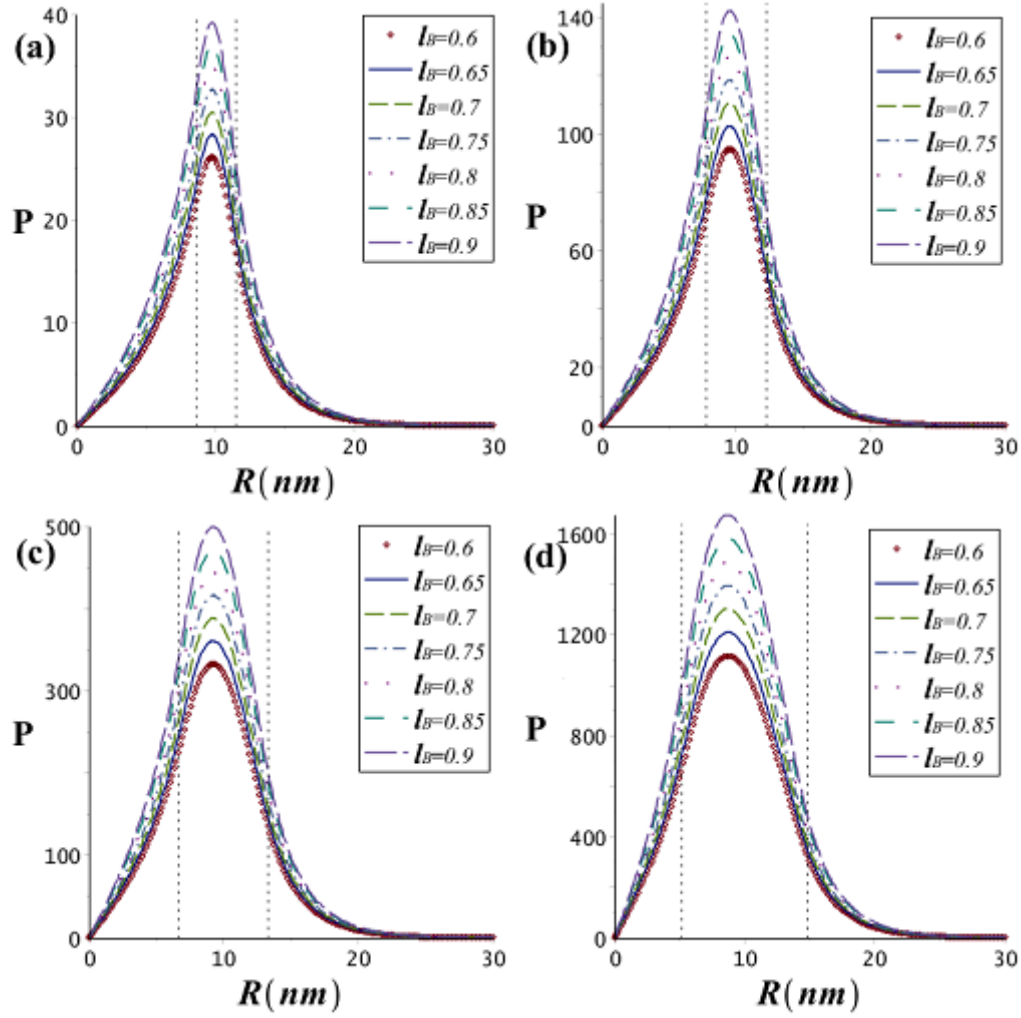


Figure 3.14: The interaction force $P(R)$ of a sphere with radius $a = 10\text{nm}$ and $Z=10,000$ immersed in a monovalent aqueous solution with 10mM concentration and Bjerrum length takes different values $l_B = 0.6, 0.65, 0.7, 0.75, 0.8, 0.85, 0.9\text{nm}$ in each case at room temperature interacts with (a) G_2 (b) G_4 (c) G_6 (d) G_8 .

The interaction maximum force values are determined by derivation ($\frac{dP}{dR} = 0$), the maximum values increase linearly with increasing Bjerrum length (l_B) in nm unit for both Cases (nano, micro sphere), (see figures (3.15),(3.18)).

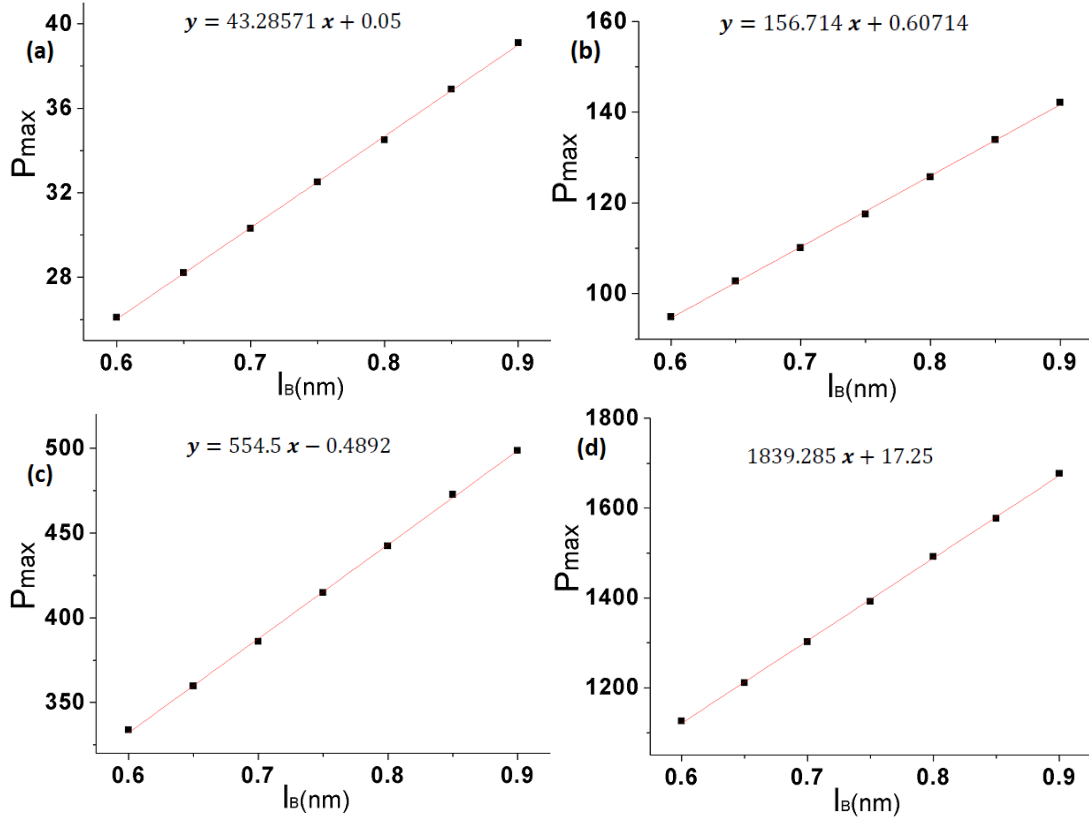


Figure 3.15: The maximum interaction force P_{\max} versus Bjerrum length l_B in (nm) unit when a sphere with 10nm radius and Charge number $Z=10,000$ interacts with (a) G_2 (b) G_4 (c) G_6 (d) G_8 .

In cases where the generations interacted with a charged sphere in micro scale, the intervals of penetration were shorter compared to the radius of the sphere. After penetration, the energy changed slightly. During this interval the interacting particles became one particle (see Figure 3.16).

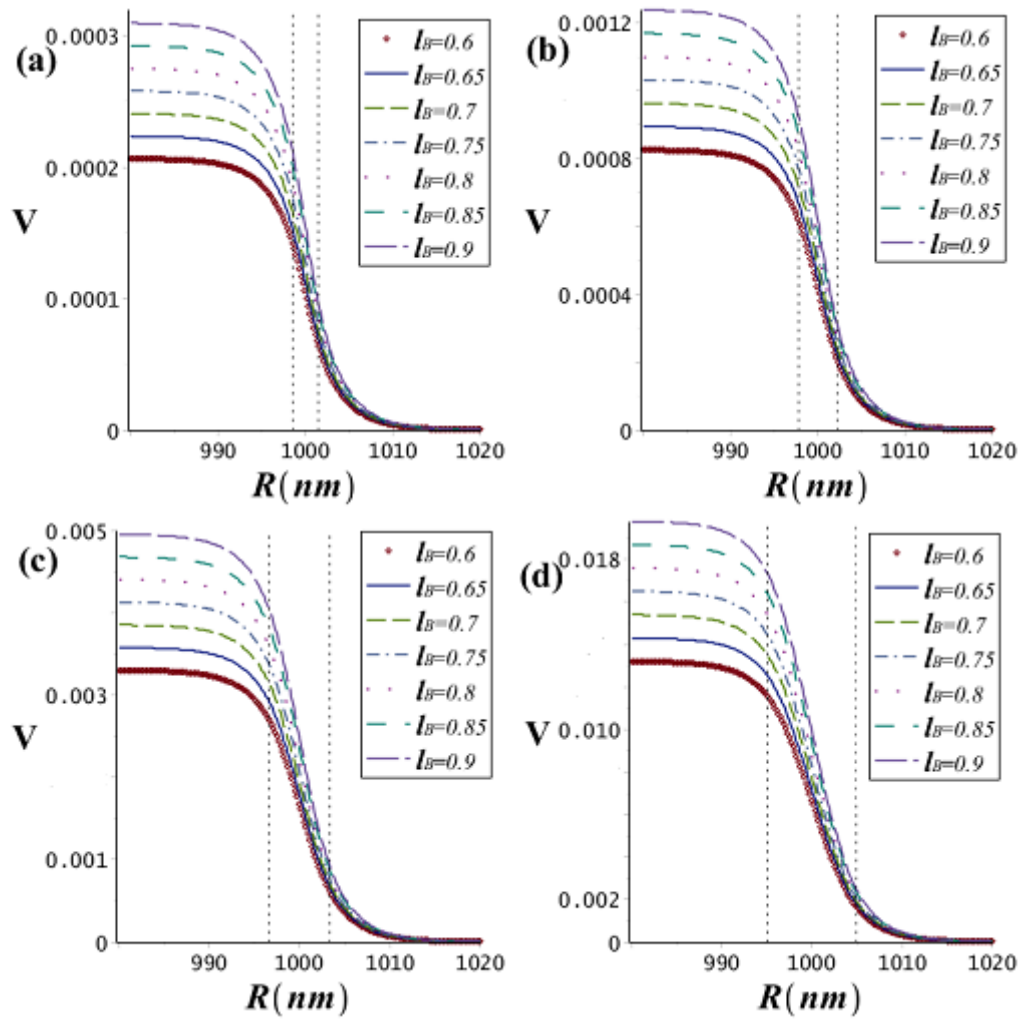


Figure 3.16: The interaction energy $V(R)$ of a sphere with radius $a = 1000\text{nm}$ and $Z=10000$ immersed in an Monovalent aqueous solution with 10mM concentration and Bjerrum length takes different values $l_B = 0.6, 0.65, 0.7, 0.75, 0.8, 0.85, 0.9\text{nm}$ in each case at room temperature interacts with (a) G_2 (b) G_4 (c) G_6 (d) G_8 .

Here, in Figure (3.17), the force curves are sharper, and symmetrical around the maximum force points.

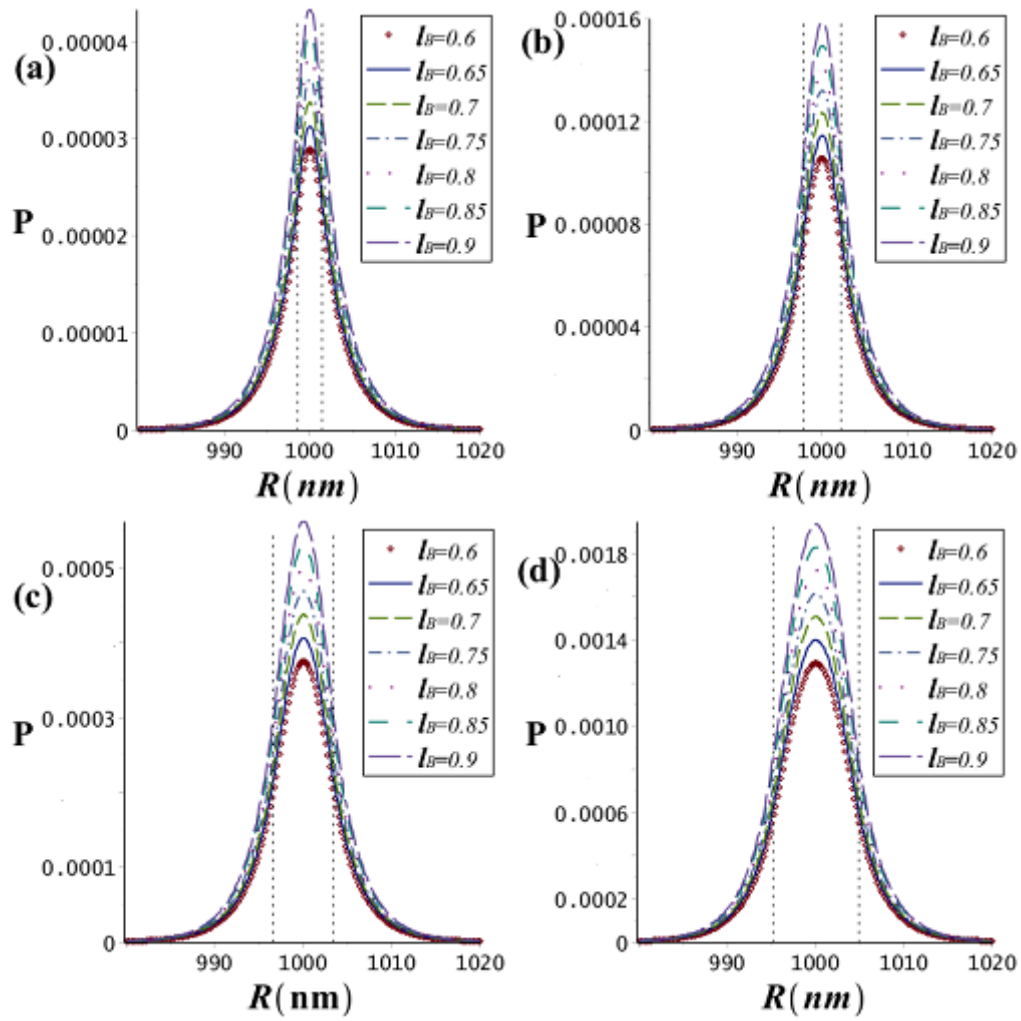


Figure 3.17: The interaction force $P(R)$ of a sphere with radius $a = 1,000\text{nm}$ and $Z=10,000$ immersed in a monovalent aqueous solution with 10mM concentration and Bjerrum length takes different values $l_B = 0.6, 0.65, 0.7, 0.75, 0.8, 0.85, 0.9\text{nm}$ in each case at room temperature interacts with (a) G_2 (b) G_4 (c) G_6 (d) G_8 .

The same behavior of maximum force values was observed where the generations of dendrimer interact with micro particle as shown in Figure (3.18).

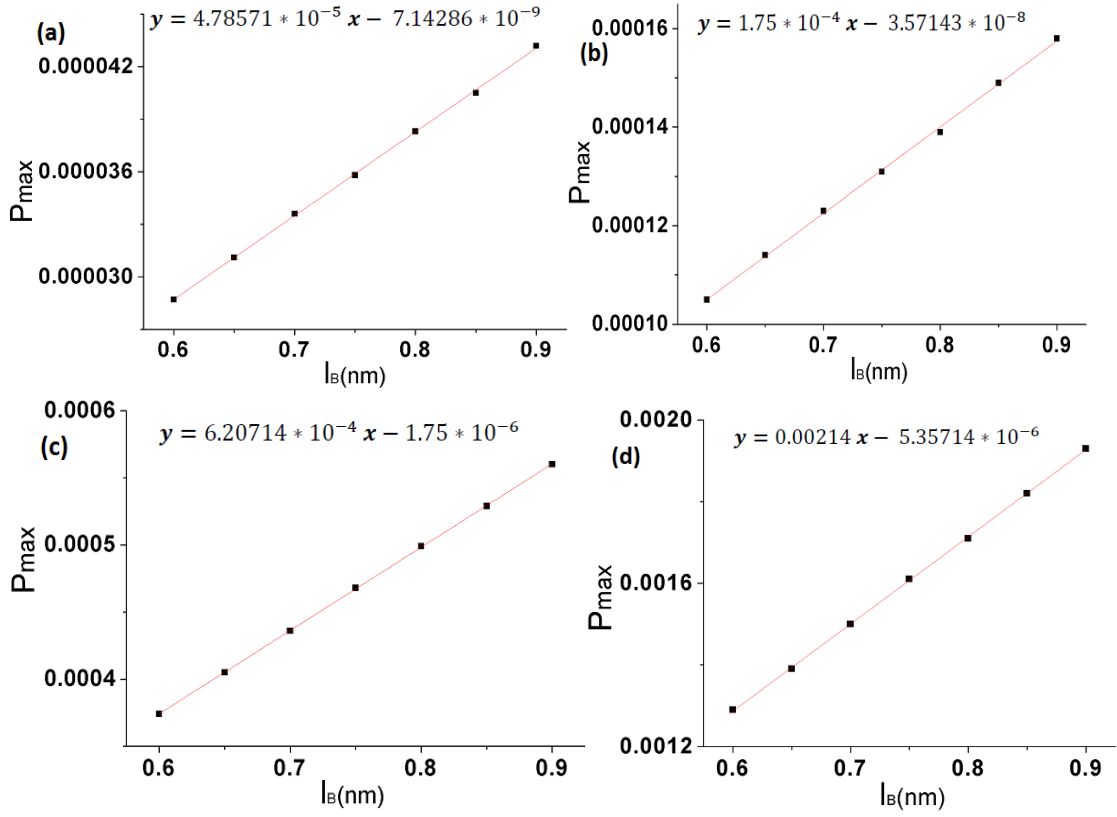


Figure 3.18: The maximum interaction force P_{\max} versus Bjerrum length l_B in (nm) unit for a sphere with 1000nm radius and charge number $Z=10,000$ interacts with (a) G_2 (b) G_4 (c) G_6 (d) G_8 .

3.2.4.2 Effect of temperature on interactions under fixed dielectric constants:

In this section the interaction energies and forces have been calculated for interaction of a soft sphere with radius 10nm, $Z=10,000$ interacts with G_2 , G_4 , G_6 , G_8 generations in monovalent salt solution with concentration 10mM, at different temperature values (T) in Kelvin. The medium of the system of the interactions could be at room temperature or at human body temperature. The values of Bjerrum length that correspond to the selected temperature values were measured as in Table 3.3. Behavior of interactions with varying temperature has been studied by using Ohshima's model as shown in figures (3.19), (3.20).

Table 3.3: Measured values of l_B under fixed relative permittivity value of water at $\epsilon_r = 80$

T (K)	278	298	318	338	358
l_B (nm)	0.75	0.7	0.66	0.62	0.58

We can see from curves of energies that the interaction energy decreases with increasing temperature T in Kelvin, (see Figure 3.19).

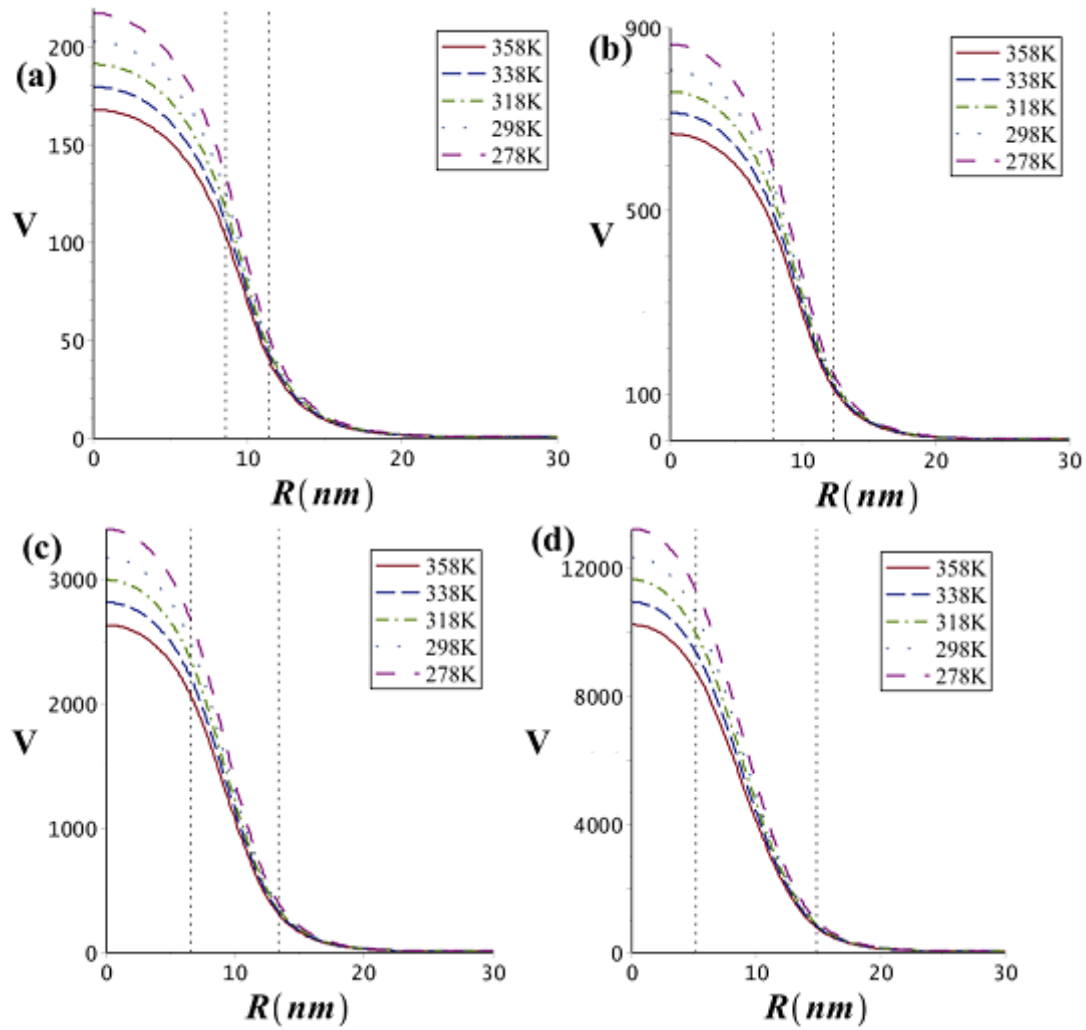


Figure 3.19: The interaction energy $V(R)$ of a sphere with radius $a = 10$ nm and $Z = 10,000$, immersed in a monovalent aqueous solution with 10 mM concentration at different values of temperature in Kelvin in each case, interacts with (a) G_2 (b) G_4 (c) G_6 (d) G_8 .

Most of the interaction changes with varying temperature happened and were observed in the penetration region, which can be explained by increasing the volume charge density during this interval. The interaction energies were increased slightly with increasing temperature during the first and second stages of interaction comparing with the third stage (engulfed stage), as shown in Figures (3.19), (3.20).

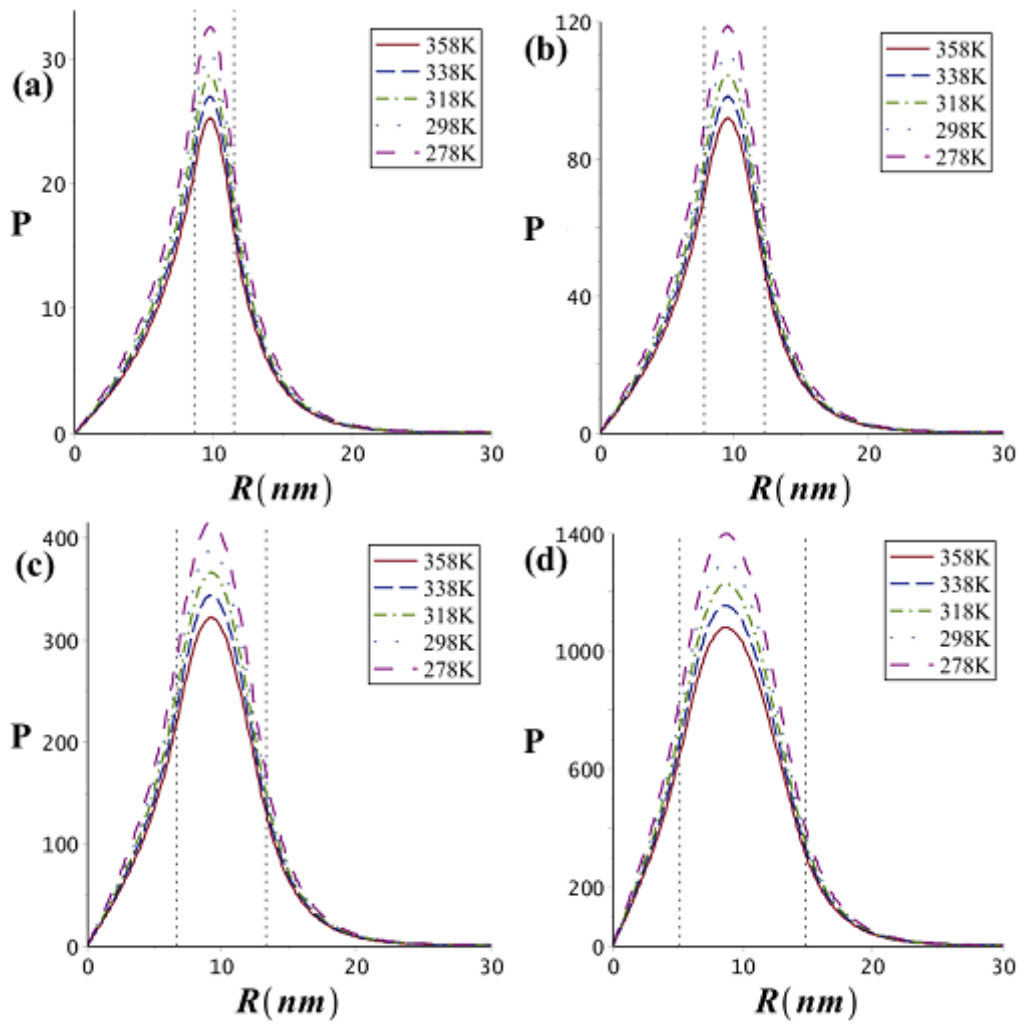


Figure 3.20: The interaction force $P(R)$ of a sphere with radius $a = 10\text{nm}$ and $Z=10,000$, immersed in a monovalent aqueous solution with 10mM concentration at different values of temperature in Kelvin in each case, interacts with (a) G_2 (b) G_4 (c) G_6 (d) G_8 .

The maximum force values were calculated by deriving ($\frac{dP}{dR} = 0$), the maximum force values increase linearly by decreasing temperature T in Kelvin as shown in Figure (3.21).

The absolute value of the slope m increases by increasing the order n of generation G_n .

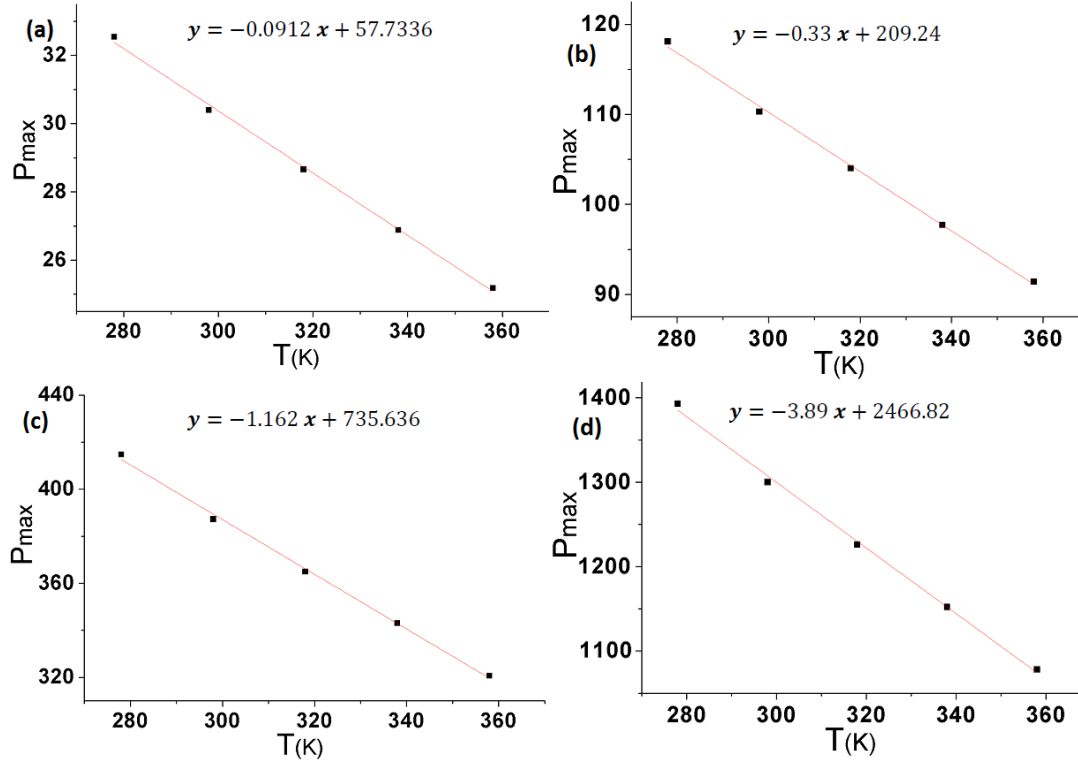


Figure 3.21: The maximum interaction force P_{\max} of a sphere with radius $a = 10\text{nm}$ and $Z = 10,000$, immersed in a monovalent aqueous solution with 10mM concentration at different values of temperature in Kelvin in each case, interacts with (a) G_2 (b) G_4 (c) G_6 (d) G_8 .

3.3 The interaction of a soft sphere with two different types of PAMAM dendrimers :

The interaction energies and forces are calculated and compared for five different generations of dendrimers for two types, Ethylenediamine cored (E.C), and Ammonia cored (A.C.) PAMAM dendrimers. Under the same conditions, we can see from figures (3.22)(3.23) that the Ethylenediamine cored dendrimer has the highest interaction energies and forces for all generations (G_2 , G_4 , G_6 , G_8 and G_{10}) compared with the Ammonia cored PAMAM dendrimer, which can be explained by the differences in volume charge densities of the two types; they have almost the same size measurements but different charge numbers for all generations (See Table 1.1).

The interactions of the two types (E.C.P, A.C.P) dendrimers with a soft sphere in nano scale (like nano drug substances, proteins, etc.) and with another soft sphere with radius in micro scale (like red blood cells,) into a salt solution with 10 mM concentration at room temperature were calculated by using Oshima's model for generations G_2 , G_4 , G_6 , G_8 and G_{10} .

The interaction energies increase clearly throughout the bounded area by the vertical colored lines, which represent the penetration limits regions of the interactions as shown in the figures (3.22)(3.23). We can explain the changes of interactions during this interval depending on the changing of volume charge density where it reaches the maximum value during the penetration region .

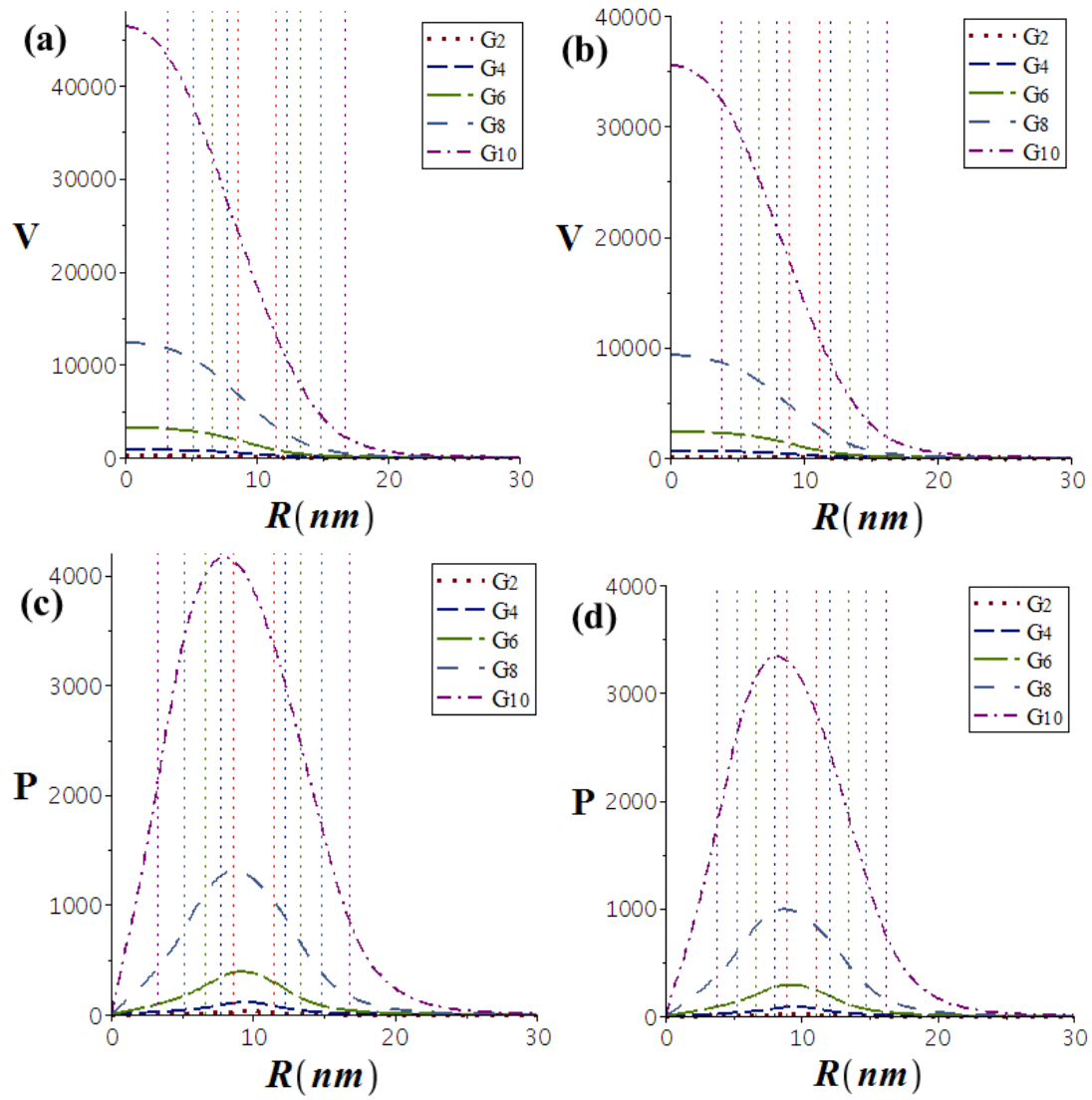


Figure 3.22: The interaction energy $V(R)$ of a sphere with radius $a = 10$ nm and $Z = 10,000$ immersed in a monovalent aqueous solution ($l_B = 0.7$) and 10mM salt concentration interacts with G_2, G_4, G_6, G_8 and G_{10} of (a) Ethylenediamine cored PAMAM dendrimer (b) Ammonia cored PAMAM dendrimer (c) Interaction force $P(R)$ for each case of (a) (d) Interaction force $P(R)$ for each case of (b)

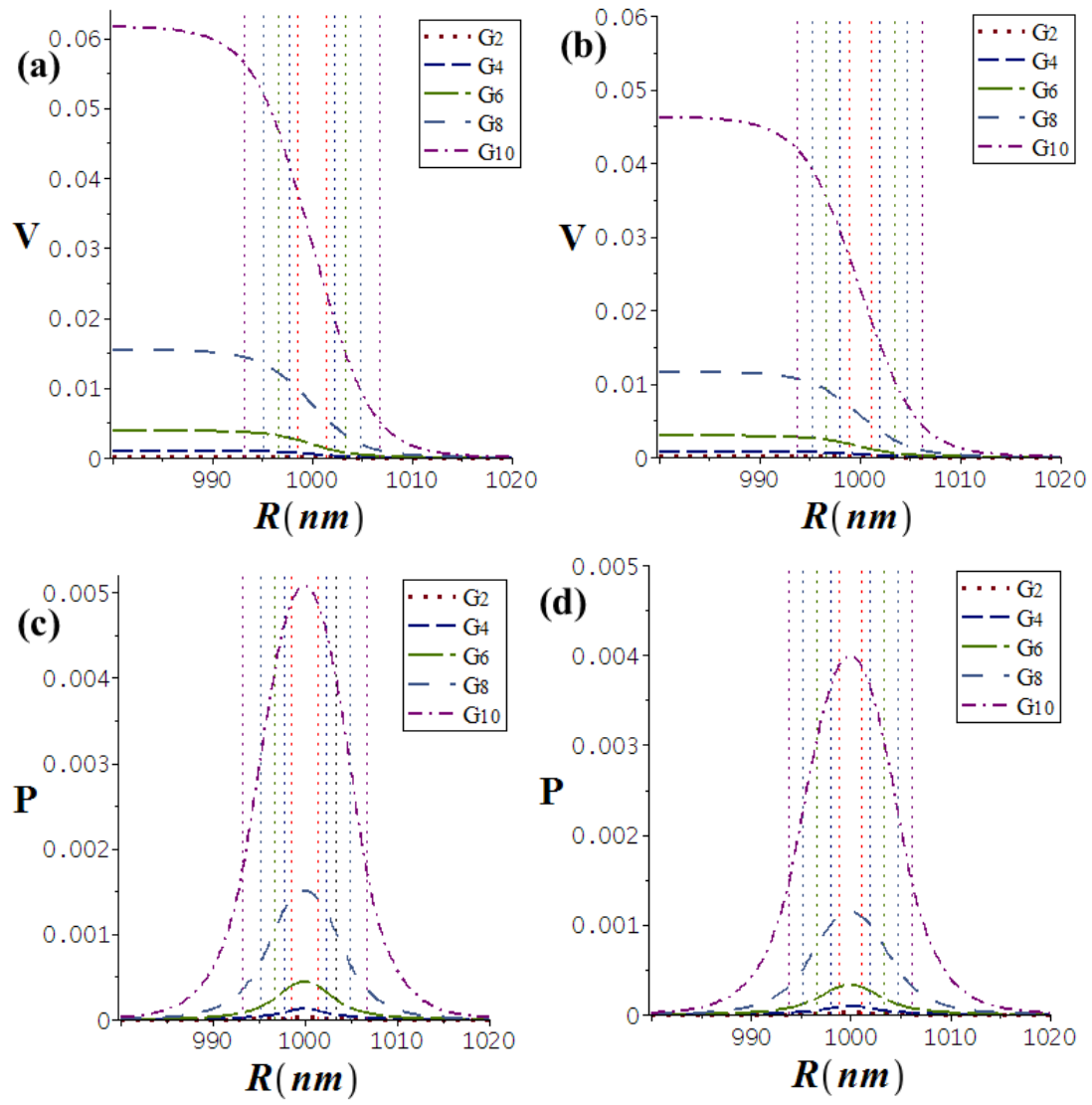


Figure 3.23: The interaction energy $V(R)$ of a sphere with radius $a = 1,000$ nm and $Z = 10,000$ immersed in a monovalent aqueous solution ($l_B = 0.7$) and 10 mM salt concentration interacts with generations G_2 , G_4 , G_6 , G_8 and G_{10} of (a) Ethylenediamine cored PAMAM dendrimer (b) Ammonia cored PAMAM dendrimer (c) Interaction force $P(R)$ for each case of (a) (d) Interaction force $P(R)$ for each case of (b).

3.4 Interactions of Complex G_n /DNA with soft charged particles :

The interaction energies and forces of a soft charged sphere with Complex G_n /DNA (where $n=4$, and 6 in this section) have been studied; the net charge of the complex is determined by the degree of DNA wrapping length (l). The dendrimer may be overcharged (*i.e.*, the net charge of the complex is negative) or undercharged (the complex has a positive charge). The net charge of the complex could be calculated by using the following formula:

$$Z_{compl} = (Z_{dend} - \frac{l}{b})e \quad \dots\dots\dots (3.1)$$

where Z_{compl} is the net charge of the complex, Z_{dend} is the charge number of the dendrimer, and the ratio $\frac{l}{b}$ represents the linear charge density of the DNA, b is the charge spacing between monomers on DNA which equals to 0.17nm (Qamhieh et al., 2009). Table 3.4 represents the calculated net charge values of two complexes G_4 /DNA and G_6 /DNA for several values of DNA wrapping length around dendrimer.

Table 3.4: The calculated net charge of complexes G_4 /DNA and G_6 /DNA , l takes the values :20, 50, 100, 150, and 200 nm, where Z_4^* is the net charge of the G_4 /DNA complex and Z_6^* is the net charge of the G_6 /DNA complex .

$l(\text{nm})$	20	50	100	150	200
Z_4^*	-50	-212	-471	-701	-880
Z_6^*	130	-36	-310	-583	-852

During the formation of complex of DNA with dendrimer, the dendrimer may show some contraction and penetration of DNA through it, hence, the radius of the complex can be approximated to the radius of dendrimer (see Table 1.1).

The interaction between complex and soft spheres can be attractive or repulsive depending on the wrapping length of DNA around the dendrimer, for example in the case of $l = 20$ nm with G_4 /DNA complex interaction being repulsive, where in with G_6 /DNA complex the interaction is attractive. The interaction energies are shown in figures (3.22) and (3.23).

When the wrapping length wraps more and more around the dendrimer, the interaction energies purely repulsive and increase by increasing of the wrapping length of DNA (l).

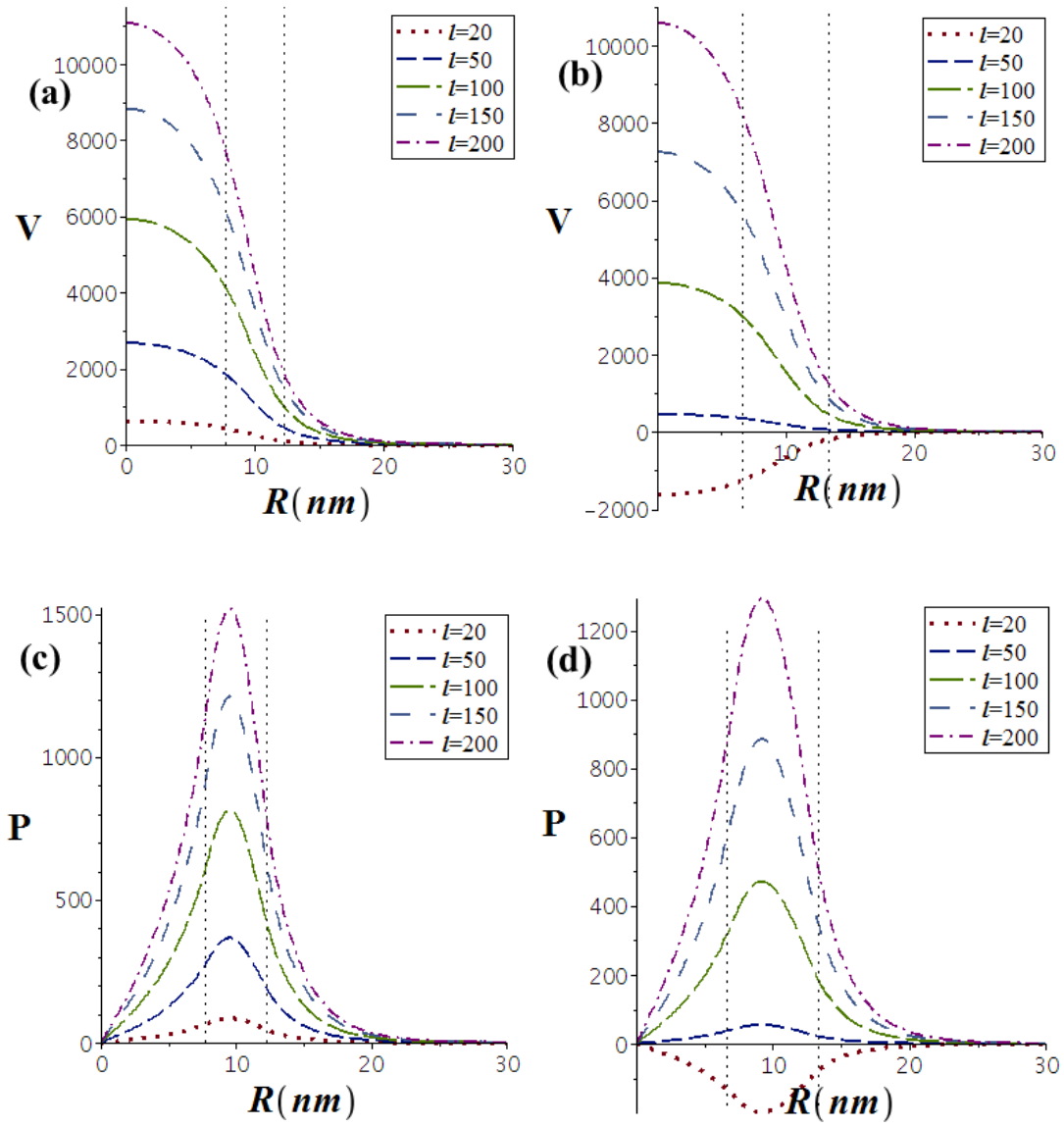


Figure 3.24: The interaction energy of a charged sphere has radius $a = 10\text{nm}$ and $Z = -10000$ immersed in a monovalent aqueous solution ($l_B = 0.7$) and 10mM salt concentration interacts with (a) Complex G_4/DNA when wrapping length of DNA (l) takes different values (b) Complex G_6/DNA (c) The interaction force in each case of a (d) The interaction force in each case of b

Similarly, the interaction energies and forces between complexes and micro scale particles (for example cells) are calculated as shown in Figure (3.25). It is clearly the values of the energies and forces for the interaction between complexes and micro scale particle is smaller than that for the interaction between complexes and nano scale particle. These differences could be explained in the following way:

The same number of charge is distributed over different volumes, hence, the charge density is the highest for smallest size.

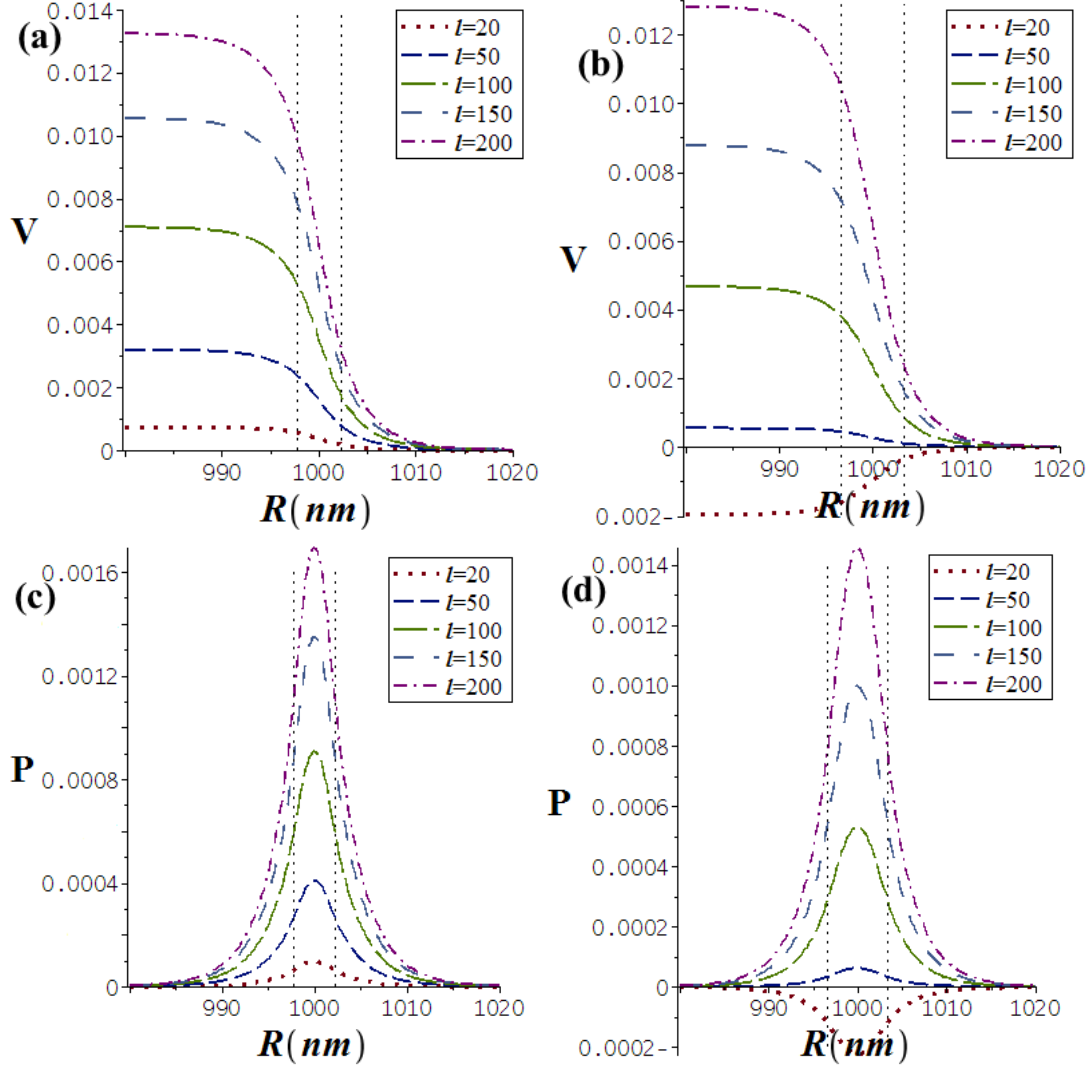


Figure 3.25: The interaction energy of a charged sphere has radius $a = 1000$ nm and $Z = -10000$ immersed in a monovalent aqueous solution ($l_B = 0.7$) and 10 mM salt concentration interacts with (a) Complex G_4 /DNA when wrapping length of DNA (l) takes different values. (b) Complex G_6 /DNA (c) The interaction force in each case of a (d) The interaction force in each case of b.

3.5 Interaction of a soft sphere with aggregates :

The aggregate consists of number (N) of complexes G_n /DNA particles, by assuming that each aggregate occupies a spherical volume, we can calculate the radius of the aggregate (r^*) by calculating the volume of the complex G_n /DNA, then multiply it by the number N to get the size of all complexes occupied in a cube of volume given by d^3 , (where d is the side length of the cube), which is given by:

$$d^3 = (4\pi/3) (N) r^3 \dots\dots\dots(3.2)$$

Where r is the radius of generation of dendrimer G_n , here, we assumed the radius of the complex approximately equals to the radius of the dendrimer of generation G_n . By assuming that there is a sphere around the cube has a radius (r^*) equals to the half of the space diagonal of the cube given by:

$$r^* = \sqrt{3/4} d \dots\dots\dots(3.3)$$

By equating equation (3.2) with (3.3), hence, the radius of the aggregate (r^*) can be written as :

$$r^* = \left(\sqrt{\frac{3}{4}}\right) [(4\pi/3) (N)]^{1/3} (r) \dots\dots\dots(3.4)$$

By simplification we get:

$$r^* = 1.4 N^{1/3} r \dots\dots\dots(3.5)$$

We can use equation (3.5) to calculate the approximate radius of the aggregate for different G_n /DNA complexes, Khawla and coworkers have calculated the theoretical values of total number of the G_n /DNA aggregates (N) and the net charge of the aggregate (Z^*e) (Qamhieh et al., 2014). Table 3.5 shows some of the theoretical values of N and Z^*e related to the number of generations G_2, G_4, G_6, G_8 .

Table 3.5: The calculated approximate radius of the aggregate of N G_n /DNA complexes, where Z^* is the net charge on the aggregate, the Z^* and N values were obtained from previous study (Qamhieh et al., 2014).

aggregate	G_2 /DNA	G_4 /DNA	G_6 /DNA	G_8 /DNA
Z^*	-3498	280	-4563	-3539
N	318	140	16	5
r^* (nm)	13.9	16.4	11.8	11.6

We applied the theoretical values of r^* and Z^* as shown in the previous table to calculate the interaction energies and forces for a system of a negative charged soft sphere of radius 50 nm and charge number 10,000 with G_n /DNA aggregates of radius r^* and Charge number Z^* by using Ohshima's model. From Figure (3.24) we can notice that the G_8 /DNA and G_2 /DNA aggregates show the same interactions and the G_6 /DNA aggregate has the highest interaction energy compared with other aggregates, which can explained that it has the largest net charge and charge density of them all. The interaction energy and force in the case of G_4 /DNA is attractive because of the different sign of the G_4 /DNA aggregate (has a positive net charge).

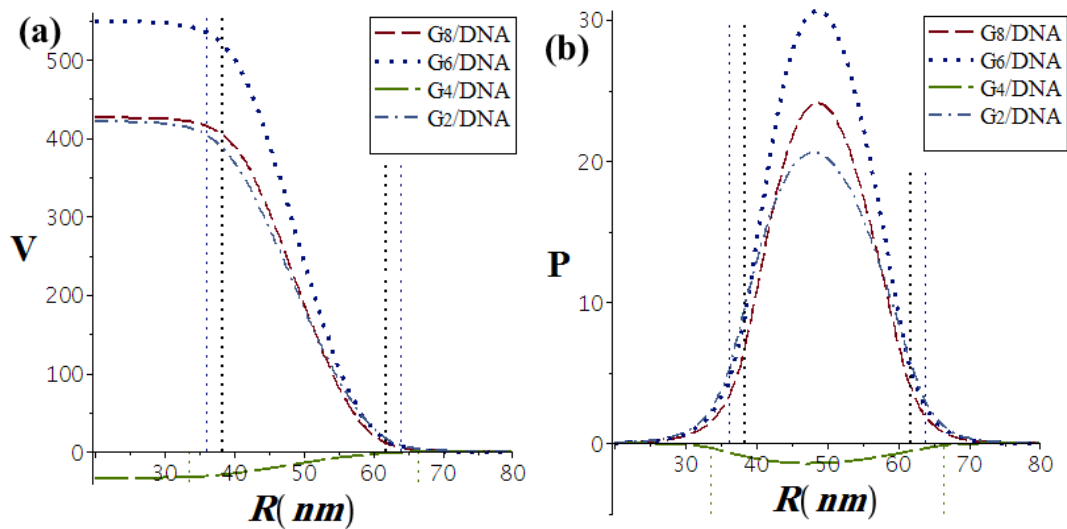


Figure 3.26: (a) The interaction energy of a charged sphere of radius $a = 50$ nm and $Z = -10000$ immersed in monovalent aqueous solution ($l_D = 0.7$) with 10 mM salt concentration interacts with different generation of aggregates. (b) The interaction force in each case of a

The interaction energies and forces of a sphere in micro scale with the G_n /DNA aggregates also were calculated (see Figure 3.24). We can notice that the behavior for all aggregates is similar to the one obtained earlier, in addition to the one mentioned above. We focus our attention on the penetration region, which shows the active region where the most changes in the interactions occurred, compared with the before and after penetration stages.

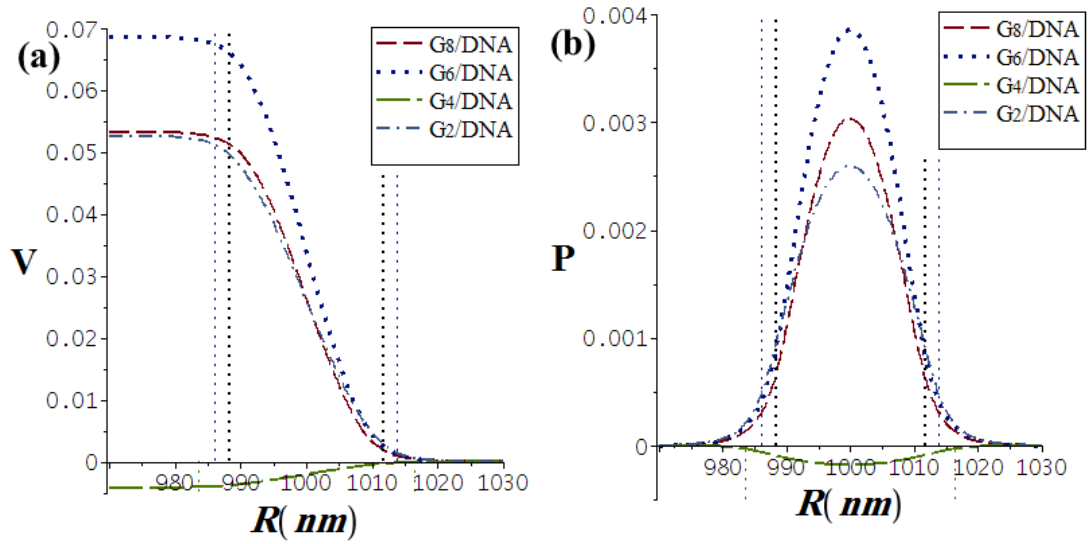


Figure 3.27: (a) The interaction energy of charged sphere of radius $a = 1,000$ nm and $Z = -10,000$ immersed in monovalent aqueous solution ($l_B = 0.7$) with 10 mM Salt concentration interacts with different generation of aggregates. (b) The interaction force in each case of a.

Chapter Four

Conclusion and Future Work

Chapter Four

Conclusion and Future Work

The analytical study presented here is the first theoretical study of the interactions between generations G_2 , G_4 , G_6 , G_8 of PAMAM dendrimers, including their complexes, and a soft charged sphere in nano and micro scale in salt solution with certain concentrations in mM unit. This study was based on a model for interactions between soft interpenetrating spheres derived by Ohshima (Ohshima, 2013). Throughout this study we concentrated on some factors that generally effect the interaction between two soft charged penetrating particles, namely, charges and sizes. We studied the maximum interaction force, and we observed no shift of the maximum by varying the charges of the interpenetrating particles. However, we found that a shift of maximum interaction force occurs by varying the sizes of the interpenetrating particles. We determined that the maximum occurs during the second third of the penetration interval.

Some parameters of the interaction between the dendrimers of different generations (G_2 , G_4 , G_6 , G_8) and other soft particles in salt solution have been studied, namely, the concentration of solvent, valence of ions, relative permittivity of solvent, and temperature in Kelvin units. We found that the maximum interaction force linearly decreases with relative permittivity and temperature in both cases (nano and micro particles).

The maximum interaction force values decrease according to the function $(m + dx^c)^{-1}$ through increasing the concentration of the solvent in Case 1 (interaction between the dendrimer generations and a nano particle). But in Case 2 (interaction between the dendrimer generations and a micro particle), the maximum interaction force values are shown to be changed, as described by the function ax^{-b} .

The interaction of two types of PAMAM dendrimers and soft charged particles have been studied and compared, the Ethylenediamine cored PAMAM dendrimer (E.C.P) shows higher interactions than the Ammonia cored PAMAM dendrimer (A.C.P) type.

Finally, we have shown that the interactions between the G_n /DNA complexes and charged soft particles of different sizes and charges are affected by varying the wrapping length of DNA around the dendrimer. In other words, the wrapping length and the dendrimer generation are important to determine the type of net charge of G_n /DNA complex, which is an important factor to identify its interaction with other charged soft particles.

Although the results presented here have demonstrated the effectiveness of Ohshima's Model, it could be further developed in a number of ways such as :

Extending Ohshima's model with other parameters

The proposed model by Ohshima could be modified by adding some parameters related to the nature of interaction medium and the soft particles, like the blood viscosity and the permittivity of human cells, etc., to obtain more reliable results. This would lead to a better global optimization for medical applications.

Extending Ohshima's model to work on a number N of interpenetrating charged spheres

In principle, the proposed three-stage model summary is describing and studying the penetration and calculating the interactions between two soft charged particles. But the larger variety and complexity of N soft charged interpenetrating particles data, especially the inter-scale gap between the N particle data, considerably increases the difficulty of the

estimation and calculation for N particles. Ohshima's three-stage model has not yet been implemented for the interaction of N interpenetrating particles.

Deriving a new model would be an extension of the work of Ohshima

Possibly, we could derive a new model by modifying the basic assumptions and conditions that Ohshima has used to derive his model (the three-stage model), for example the relative permittivity. Ohshima assumed that the relative permittivity in spheres 1 and 2 take the same value ϵ_r as that of the electrolyte solution. Instead, it would be more realistic to assume that the relative permittivity of the electrolyte solution takes a different value than the sphere's values. For example, in experiments using water as a medium of interaction (for example aqueous solution), the measured value of the relative permittivity is around 80, while on the other hand, the other particles – for example the PAMAM dendrimer – has a measured relative permittivity value around 2.

There is clearly much work to be done in the area of developing Ohshima's three-stage model. Perhaps the most direct extension of this work is to hypothesize about how best to develop a more precise knowledge of the interaction between soft particles, thus opening the door for other researchers to cope with ambiguities at branch points, like the interaction between dendrimers and cells or between cells and proteins. This will benefit the field of gene therapy.

References

- Ainalem, M-L., Nylanderet, T., (2011), DNA condensation using cationic dendrimers morphology and supramolecular structure of formed aggregates, *Soft Matter*, 7, 4577-4594.
- Bruckman, M.A, Yu, X., Steinmetz, N. F, (2013), Engineering Gd-loaded nanoparticles to enhance MRI sensitivity via T1 shortening, *Nanotechnology*, 24, 46.
- Buhleier, E., Wehner, W., Vögtle, F., (1978), Syntheses of Molecular Cavity Topologies, *Synthesis* 1978, 2, 155-158.
- Butt, H., (1991), Electrostatic interaction in atomic force microscopy, *Biophysical Journal*, 60, 777-785.
- Dähnert, K., Rödenbeck, M., (1994), Exact Solution of Bisphere DEBYE-HÜCKEL Problem, *Journal of Colloid and Interface Science*, 163, 229-233
- Dennig, J., Duncan, E., (2002), Gene transfer into eukaryotic cells using activated polyamidoamine dendrimers, Elsevier Science
- Ducker, W., Senden, A., Pashley, T. J., (1991), *R. M. Nature*, 353, 239-241.
- Eichman, J.D., Bielinska, A.U., Kukowska-Latallo, J.F., and Baker, J.R., (2000), The use of PAMAM dendrimers in the efficient transfer of genetic material into cells, 3,7.
- Evans, M., Ahmad, A., Ewert, K., Pfohl, T., Martin-Herranz, A., Bruinsma, R. F., and Safinya, C. R., (2003), Structural polymorphism of DNA-dendrimer complexes, Vol.91.
- Ferenc, M., Pedziwiatr-Werbicka, E., Nowak, K.E., Klajnert, B., Majoral, J-P., and Bryszewska, M., (2013), Phosphorus Dendrimers as Carriers of siRNA Characterisation of Dendriplexes, *Molecules*, 16, 4451-4466.
- Hawker, C. J., Fréchet, J. M. J., (1990), Preparation of polymers with controlled molecular architecture. A new convergent approach to dendritic macromolecules, *Chem. Soc.*, 112, 7638.
- Holister, P., Vas, C. R., Harper, T., (2003), *Dendrimers*, Cientifica .
- Kabanov, V. A., Sergeyev, V. G., Pyshkina, O. A., Zinchenko, A. A., Zezin, A. B., Joosten, J. G. H., Brackman, J., Yoshikawa, K., (2000), Interpolyelectrolyte Complexes Formed by DNA and AstramolPoly (propylene imine) Dendrimers, *Macromolecules*, 33, 9587-9593.
- Kornberg, R.D., Lorch, Y., (1999), Twenty-Five Years of the Nucleosome Fundamental Particle of the Eukaryote Chromosome, *Cell*, Vol.98, 285-294.

- Lee, H, Larson, R.G., (2009), Multiscale Modeling of Dendrimers and Their Interactions with Bilayers and Polyelectrolytes, *Molecules*, 14, 423-438.
- Li, Y. Q., Tao, N. J., Pan, J., Garcia, A. A., Lindsay, T-S. M., (1993), Direct Measurement of Interaction Forces between Colloidal Particles Using the Scanning Force Microscope, *Langmuir*, 9, 637-641.
- Mateescu, E. M., Jeppesen, C., Pincus, P., (1999), Overcharging of a spherical macroion by an oppositely charged polyelectrolyte, *Europhys. Lett.*, 46, 493.
- Messina, R., Holm, C., Kremer, K., (2013), Strong electrostatic interactions in spherical colloidal systems, *Max-Planck-Institut*, 10, 55128.
- Ohshima, H., (2008), Electrostatic interaction between soft particles, *Journal of Colloid and Interface Science*.
- Ohshima, H., (2013), Electrostatic interaction between two interpenetrating soft particles, *Journal of Colloid and Interface Science*.
- Ohshima, H., (2010), *Biophysical Chemistry of Bio interfaces*, John Wiley & Sons, p. 96.
- Ohshima, H., (2010), *Biophysical Chemistry Of Bio interfaces*, John Wiley & Sons, pp.306-310.
- Patil, M. L., Zhang, M., Betigeri, S., Taratula, O., He, H., and Minko, T., (2008), Surface Modified and Internally Cationic Polyamidoamine Dendrimers for Efficient siRNA Delivery, *Bioconjugate Chem*, 19, 1396–1403.
- Qamhieh, K., Nylander, T., Black, C. F., Attard, G. S., Dias, R. S., and Ainalem, M –L., (2014), Complexes formed between DNA and poly(amidoamine) dendrimers of different generations modelling DNA wrapping and penetration, *Physical Chemistry Chemical Physics*.
- Qamhieh, K., Nylander, T., and Ainalem, M.-L., (2009), *Biomacromolecules*, 10, 1720-1726.
- Qamhieh, K., Nylander, T., Black, C. F., Attard, G. S., Dias, R. S., and Ainalem, M-L., Complexes Formed between DNA and Poly(amido amine) Dendrimers of Different Generations – modelling DNA wrapping and penetration.
- Qamhieh, K., Khaleel, A. A., (2013), Analytical model study of complexation of dendrimer as an ion penetrable sphere with DNA, *ScienceDirect*.
- Schiessel, H., Bruinsma, R. F., Gelbart, W. M., (2001), Electrostatic complexation of spheres and chains under elastic stress, *J. of chemical physics*, 115, 7245.
- Stace, A. J., Bichoutskaia, E., (2012), Absolute electrostatic force between two charged particles in a low dielectric solvent, *Soft Matter*, 8, 6210.

Szilagyi, I., Trefalt, G., Tiraferri, A., Maroni, P., Borkovec, M., (2014), Polyelectrolyte adsorption, interparticle forces, and colloidal aggregation, *Soft Matter*, 10, 2479-2502.

Thomas, M., Klibanov, A.M., (2003), Non-viral gene therapy: polycation-mediated DNA delivery, *Applied Microbiology and Biotechnology*, 62, 27-34.

Verma, A., Stellacci, F., (2009), *Effect of Surface Properties on Nanoparticle Cell Interactions*, InterScience.

الملخص

تم اعداد هذه الدراسة لتحسين وتوسيع فهم التفاعل الكهربائي بين (PAMAM) دندريمر ومتشكلاتها، دندريمر-حمض نووي (complex) ودندريمر-حمض نووي متعدد (aggregate)، وبين جسيم مشحون قابل للاختراق مثل الخلية او البروتين في محلول ملحي، تم حساب ودراسة التفاعل الكهروستاتيكي بين الجسيمات القابلة للاختراق مثل الدندريمرز و البروتين والخلية بتطبيق نموذج نظري مطور ومحدث بواسطة Ohshima يصف التفاعل بين كرتين مشحونتين قابلتين للاختراق على ثلاث مراحل، قبل، وأثناء، وبعد الاختراق. لقد وجد أن القوة الكهربائية المتبادلة القصوى بين الجسيمين المتداخلين تحدث خلال الثلث الثاني من منطقة التداخل. وأن التفاعل الكهربائي بين الجسيمين يعتمد بشكل ملحوظ على الحجم وذلك عند تغير تركيز المحلول الملحي. ووجد ان التفاعلات الكهروستاتيكية مع المتشكلات، دندريمر-حمض نووي (complex) ودندريمر-حمض نووي متعدد (aggregate)، يحددها درجة التقاف شريط الحمض النووي (DNA) حول الدندريمر. الدراسة الحالية توسع مفهومنا حول التفاعل بين الجسيمات القابلة للاختراق في العلاج الجيني.